CHAPTER 3

RESULTS AND DISCUSSION

In this thesis, the particles properties and application of unloaded TiO_2 and metal-loaded TiO_2 synthesized by FSP are discussed by XRD, SEM with EDS-dot mapping mode, HRTEM, BET analysis. Gas sensing films of all samples were tested towards flammable gases (H_2, C_2H_5OH and $(CH_3)_2CO$) and environmentally hazardous gases (SO_2 and CO).

3.1 Characterization of unloaded TiO_2 and metal-loaded TiO_2 [134–135]

3.1.1 X-ray diffraction (XRD) analysis

It can be seen that all samples were highly crystalline, and the phase of gas sensing film on flame-made unloaded TiO_2 and 0.25–3.0 mol% metal-loaded TiO_2 nanoparticles before annealing and sensing test at 400 ^oC were analyzed by XRD. The XRD spectra of unloaded TiO_2, 0.25, 0.50, 0.75, 1.0, 2.0 and 3.0 mol% metal-loaded TiO_2 nanopowders are shown in Figures 3.1 (a), (b) and (c). The diffraction peaks of the unloaded TiO_2 and metal-loaded TiO_2 samples showed similar pattern in both anatase and rutile phases of TiO_2 in all samples, which matched well with the JCPDS file No. 21–1272 and JCPDS file No. 21–1276, respectively. The XRD peaks of Pt and Ag peaks were not found in these patterns as shown in Figures 3.1 (a) and (c) because Pt (JCPDS file No. 87–0640) and Ag (JCPDS file No. 87–0717) were loaded in the range of very low concentration and Pt and Ag nanoparticles were very small, which were later proved by the HRTEM results. Au peaks were found in

these patterns (JCPDS file No. 04–0784). It can be assumed that the amount of Au concentration was very low, which affected the appearance of the Au peaks as shown in Figure 3.1 (b).

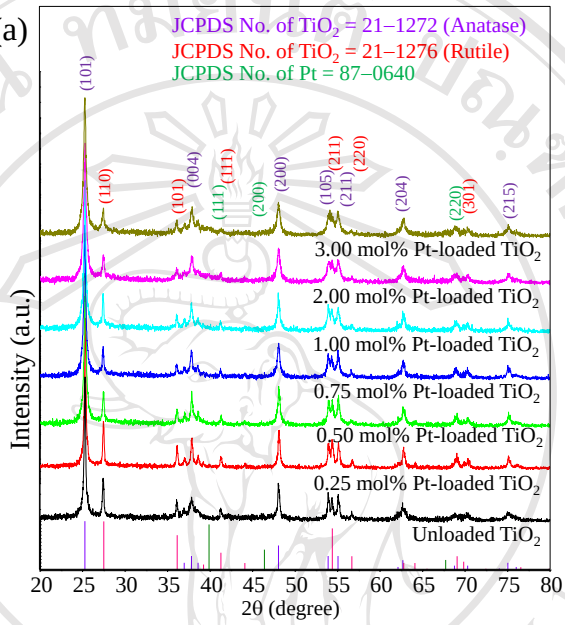

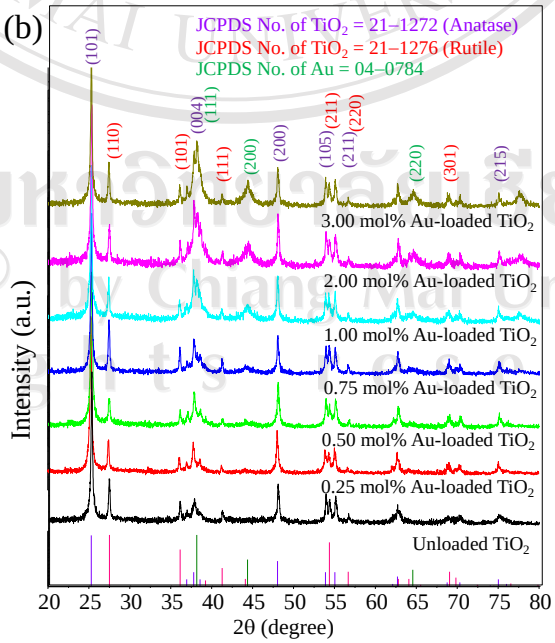

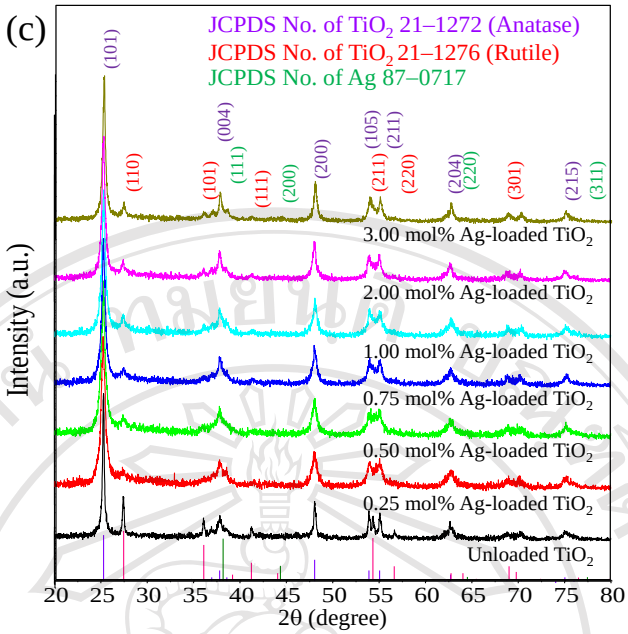

Figure 3.1 XRD patterns of flame-spray-made (5/5) unloaded TiO_2 as-prepared, 0.25, 0.50, 0.75, 1.0, 2.0 and 3.0 mol% Pt (a), Au (b) and (c) Ag-loaded TiO_2 samples.

3.1.2 Scanning electron microscopy (SEM)

The SEM images of unloaded TiO_2, (a) 0.25, (b) 0.50, (c) 0.75, (d) 1.0, (e) 2.0 and (f) 3.0 mol% Pt, Au and Ag-loaded TiO_2 nanoparticles are shown in Figures 3.2, 3.3 and 3.4, respectively. The morphology of highly crystalline flame-made (5/5) were investigated by SEM. It can be seen that nanoparticles were spherical in shape, the surface of the nanopowders porous, and well dispersed without evidence of aggregation. From this observation, it was found that the rough morphology were not changed with increasing metal loading levels, but the rough particle sizes were slightly changed with increasing metal loading levels.

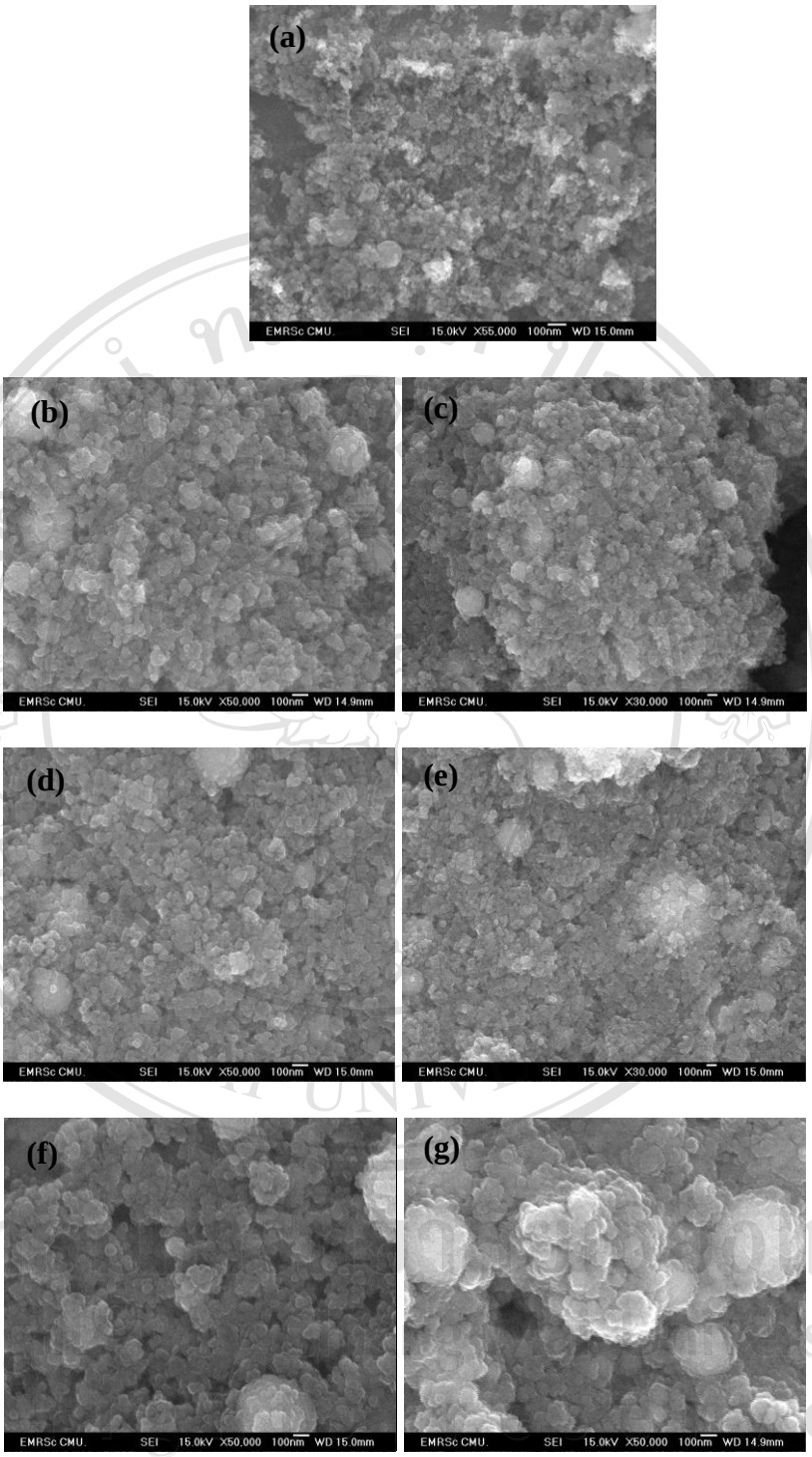

Figure 3.2 The morphology of highly crystalline flame–made (5/5) (a) unloaded TiO_2, (b) 0.25 mol% Au-loaded TiO_2, (c) 0.50 mol% Au-loaded TiO_2, (d) 0.75 mol% Au-loaded TiO_2, (e) 1.0 mol% Au-loaded TiO_2, (f) 2.0 mol% Au-loaded TiO_2 and (g) 3.0 mol% Au-loaded TiO_2 nanoparticles for SEM analysis.

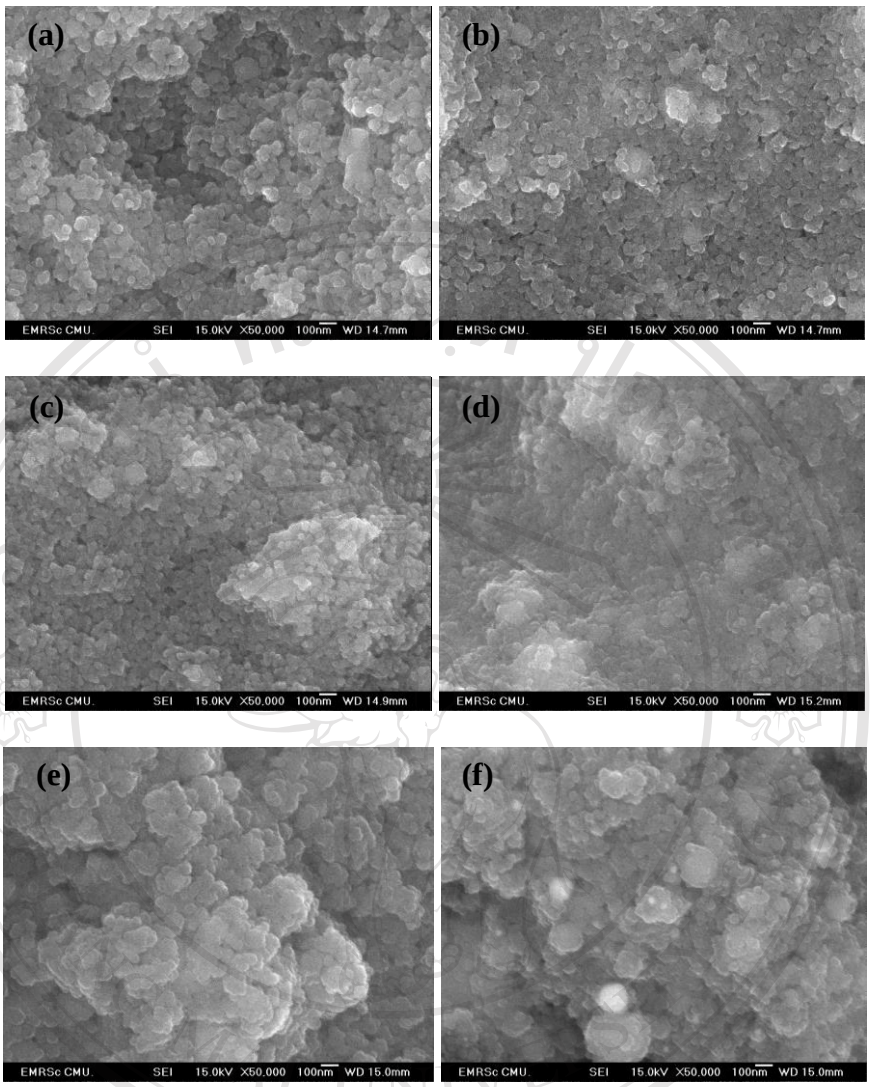

Figure 3.3 The morphology of highly crystalline flame–made (5/5) (a) 0.25 mol% Pt-loaded TiO_2, (b) 0.50 mol% Pt-loaded TiO_2, (c) 0.75 mol% Pt-loaded TiO_2, (d) 1.0 mol% Pt-loaded TiO_2, (e) 2.0 mol% Pt-loaded TiO_2 and (f) 3.0 mol% Pt-loaded TiO_2 nanoparticles for SEM analysis.

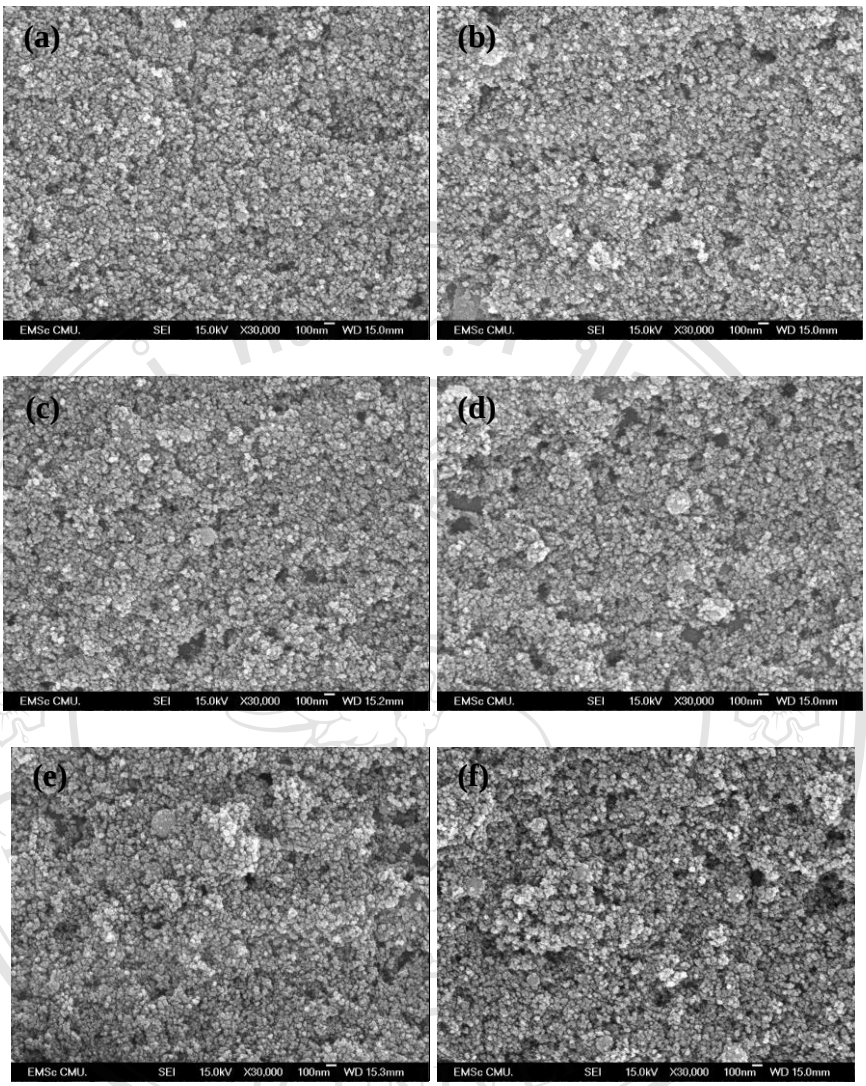

Figure 3.4 The morphology of highly crystalline flame–made (5/5) (a) 0.25 mol% Ag-loaded TiO_2, (b) 0.50 mol% Ag-loaded TiO_2, (c) 0.75 mol% Ag-loaded TiO_2, (d) 1.0 mol% Ag-loaded TiO_2, (e) 2.0 mol% Ag-loaded TiO_2 and (f) 3.0 mol% Ag-loaded TiO_2 nanoparticles for SEM analysis.

3.1.3 Energy Dispersive X-Ray Spectroscopy (EDS)

The trends in the elemental composition of the agglomerated nanoparticles formed of sample (a) unloaded TiO_2, (b) 1.0 mol% Pt-loaded TiO_2, (c) 1.0 mol% Au-loaded TiO_2 and (d) 1.0 mol% Ag-loaded TiO_2 were shown by the EDS spectra in Figures 3.5. The EDS spectra showed the elemental histograms corresponding to a rich in copper tape by the Cu substrate, poor carbon (C) caused by an C sputtering prior to the analysis, titanium (Ti), oxygen (O), poor platinum (Pt) and poor gold (Au) as shown in Figures 3.5 (a), (b) and (c). Figures 3.5 (d) showed the elemental histograms corresponding to a rich in copper tape by the Cu substrate, poor gold (Au) caused by an Au sputtering prior to the analysis, titanium (Ti), oxygen (O) and poor silver (Ag). It can be seen that Ti, O, Pt, Au and Ag elements were quite evenly distributed over the area. In addition, the density of Pt, Au or Ag sites was approximately a few percent of those of Ti and O sites.

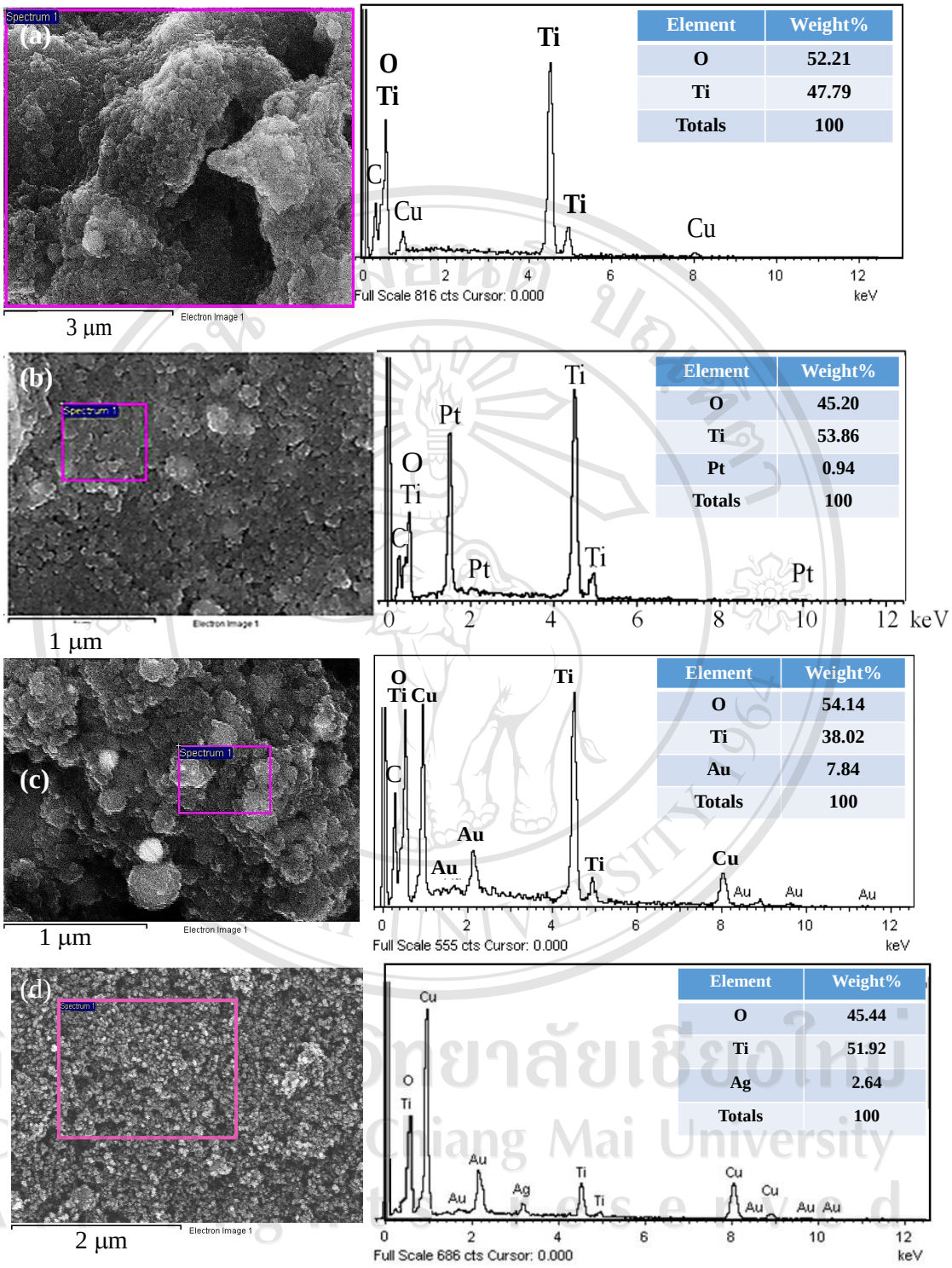

Figure 3.5 The EDS spectra images of all elements in the (a) unloaded TiO_2, (b) 0.50 mol% Pt-loaded TiO_2, (c) 1.0 mol% Au-loaded TiO_2 and (d) 1.0 mol% Ag-loaded TiO_2 nanoparticles.

3.1.4 High resolution transmission electron microscopy (HRTEM)

HRTEM bright-field images of FSP-made unloaded TiO_2 and Pt, Au and Ag-loaded TiO_2 nanoparticles with 1.0 mol% metal loadings are shown in Figure 3.6. Spherical metal nanoparticles/ clusters dispersed on the surface of TiO_2 were clearly observed as the darker spots. The unloaded TiO_2 nanoparticles and metal-loaded TiO_2 were seen as particles having a clear spherical morphology. The selected area electron diffraction (SAED) pattern of unloaded TiO_2 and metal-loaded TiO_2 in Figures 3.6 (a), (b), (c) and (d) were indexed and identified as the crystal structure, corresponding to the (101), (004), (200) and (105) crystal planes of anatase phases of unloaded TiO_2 and metal-loaded TiO_2. The SAED rutile of TiO_2 was not detected, possibly because of the different in ratio of anatase and rutile. Figure 3.6 (e) shows lattice fringes of TiO_2 sample. These lattice fringes of TiO_2 matched well with *d*-spacing of TiO_2, which were measured and identified as the crystal structure of TiO_2. The dominance of (004) and (200) planes of anatase and (110) planes of rutile structure can be used to confirm the fringe widths of 0.231 nm, 0.180 nm and 0.245 nm, respectively. The crystallite sizes of spherical unloaded TiO_2 and metal-loaded TiO_2 were found to be ranging from 10−80 nm. HRTEM images show that very small Pt, Ag nanoparticles as uniformly dispersed on the surface of larger TiO_2 particles. The size of Pt nanoparticles is smaller than 2 nm for Pt or Ag-loaded TiO_2. The average size of Au nanoparticles were 5–15 nm. The uniform metal dispersion throughout TiO_2 support is very important for enhancing the gas sensing properties of metal oxide.

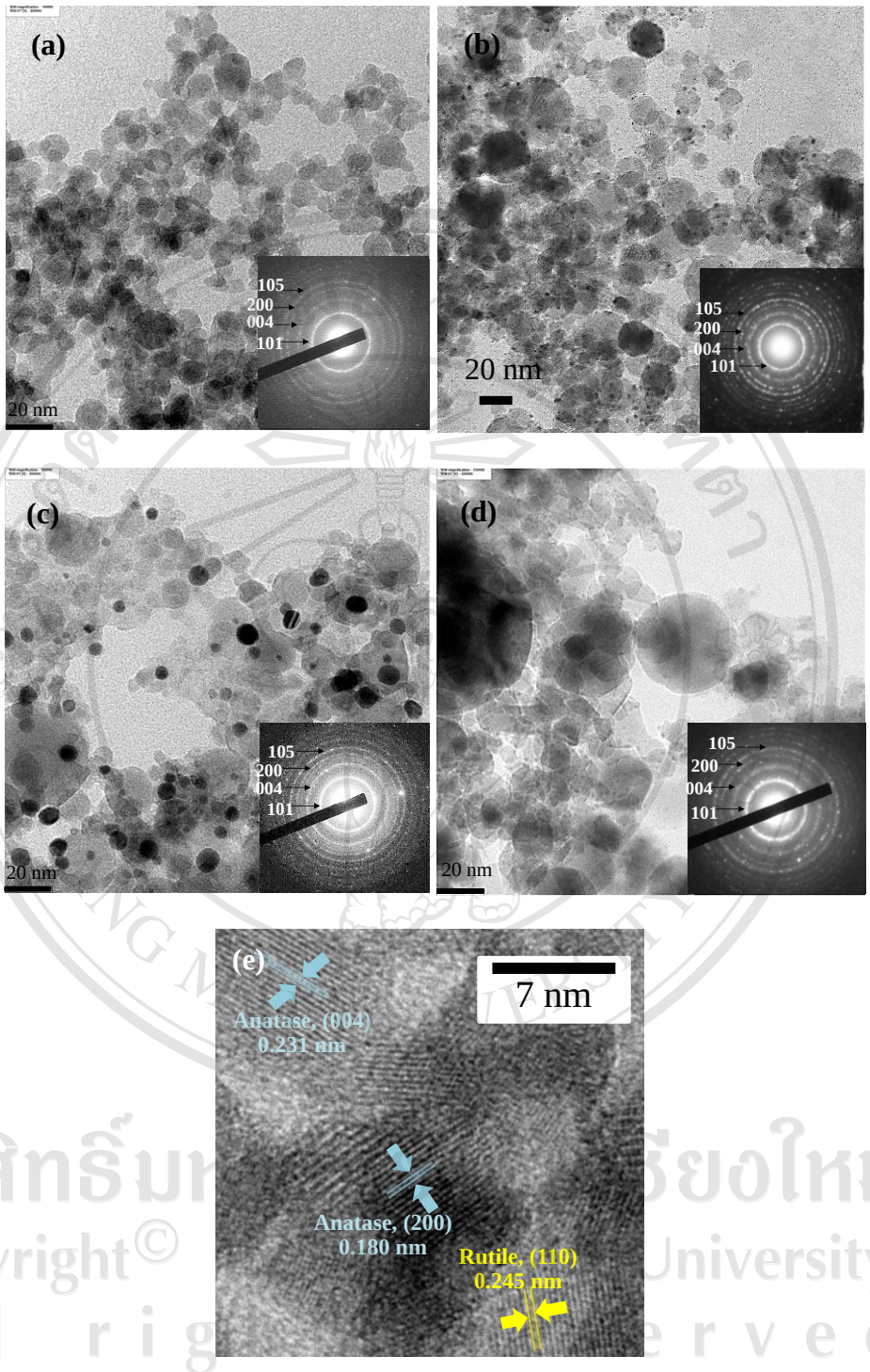

Figure 3.6 HRTEM images of (a) unloaded TiO_2, (b) 1.0 mol% Pt-loaded TiO_2, (c) 1.0 mol% Au-loaded TiO_2, (d) 1.0 mol% Ag-loaded TiO_2 and (e) lattice fringes image of TiO_2 nanoparticles.

3.1.5 BET analysis

The average BET equivalent particle diameter (d_{BET}) as shown in Figure 3.7 were calculated using the average of the density of (a) Pt, (b) Au and (c) Ag-loaded TiO_2 taken into account for their weight content of different loading. The SSA_{BET} was measured by five-point nitrogen adsorption and the d_{BET} was calculated using $d_{BET} = 6/[(\rho_{TiO_2} \times SSA_{TiO_2} \times wt\%_{TiO_2}) + (\rho_{metal} \times SSA_{metal} \times wt\%_{metal})]$ where ρ is the powder density. It can be seen that SSA_{BET} monotonically increases while d_{BET} decreases with increasing metal concentration from 0 to 3.0 mol%. The results can be explained as follows. When metal particles were formed and deposited on TiO_2 supports in the flame, metal created a new nucleation center, which in turns changed the nucleation type from homogeneous to heterogeneous. The d_{BET} of metal-loaded TiO_2 nanoparticles would be the average size of the combined Pt and TiO_2; Au and TiO_2; Ag and TiO_2 nanoparticles. With the increasing Pt, Au and Ag loading, the number of Pt, Au and Ag particles increased and hence the average particles would decrease because the size of Pt, Au and Ag nanoparticles was expected to be much smaller than that of TiO_2 nanoparticles.

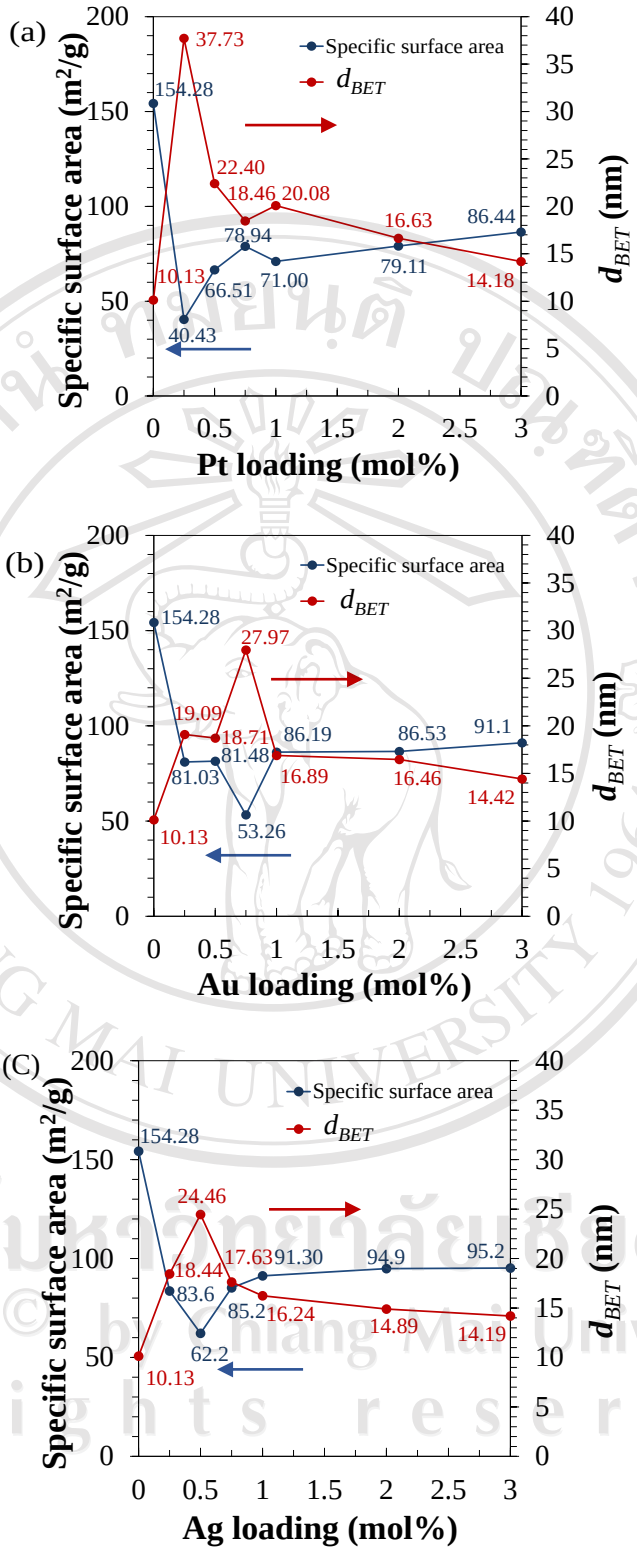

Figure 3.7 The specific surface area (SSA_{BET}) and d_{BET} of (a) Pt, (b) Au and (c) Ag-loaded TiO_2 nanoparticles.

3.1.6 Film thickness of sensing layer

The cross-section, film thickness and surface morphology of the sensing film based on flame-made nanopowders layer after annealing and gas sensing test at 400 °C were observed using SEM analysis as shown in Figures 3.8 (a), (b), (c) and (d). It was found that film thickness of unloaded TiO_2, 0.50 mol% Pt-loaded TiO_2, 1.0 mol% Au-loaded TiO_2 and 1.0 mol% Ag-loaded TiO_2 sensors were about 15, 14, 7.0 and 6.2 μm, respectively. These results could confirm that film thickness of all sensors were in the same range of about 5–15 μm. The Al_2O_3 substrates were also visible in all images. The gold electrode layers of gas sensing films were found in Figures 3.12 (a) and (c). The thicknesses of these gold electrodes were in the range of 0.1 μm.

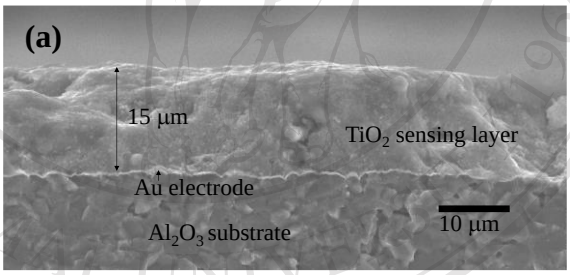

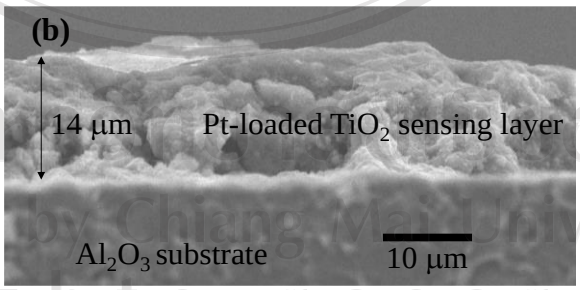

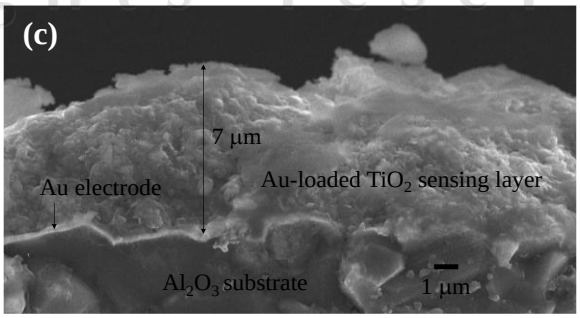

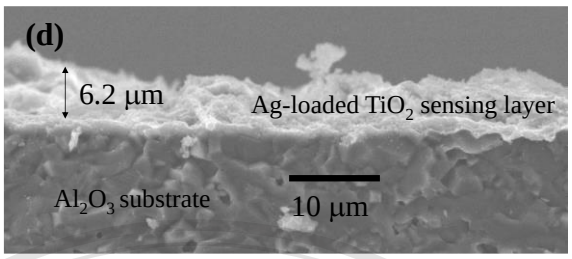

Figure 3.8 Cross-section SEM micrograph of gas sensing film based on flame made (a) unloaded TiO_2, (b) 0.50 mol% Pt-loaded TiO_2, (c) 1.0 mol% Au-loaded TiO_2 and (d) 1.0 mol% Ag-loaded TiO_2 nanoparticles.

3.2 Gas sensing properties

The gas sensing properties are characterized in terms of dynamic change of resistance and gas-sensing sensitivity. The gas sensing sensitivity of n-type semiconductor based conductometric gas sensor to a reducing gas is normally defined as the ratio, S is defined as the ratio R_a/R_g, where R_a is the resistance in dry air, and R_g is the resistance in test gas. For p-type semiconductor gas sensor, the definitions are reversed ($S = R_g/R_a$). The response time (T_{res}) is defined as the time required to reach 90% of the steady response signal. The recovery times (T_{rec}) denotes the time needed to recover 90% of the original baseline resistance. The gas-sensing sensitivity was calculated from dynamic variation of the conductance due to gas pulses introduction and plotted versus various parameters including temperature and gas concentration.

3.2.1 Gas sensing of metal-loaded TiO_2 nanoparticles synthesized by FSP towards hydrogen (H_2) gas [134–135]

Hydrogen gas is an important gas for clean energy sources, highly flammable, and burnable in air at a very wide range (4–75% by volume). However, its presence due to leakage at a sufficient high concentration together with oxygen in air will cause explosion. Moreover, H_2 cannot be detected by human senses when it leaks. Therefore, semiconducting metal-loaded TiO_2 is one of the most promising candidates for flammable gas detection due to its advantages including low cost, high sensitivity, fast response, simplicity of use, and ability to detect a large number of gases.

The interaction of the resistive sensors with analyzing H_2 gas caused a change in the resistance of the unloaded TiO_2 and metal-loaded TiO_2 sensors. Figure 3.9 shows the sensor resistance versus sensing time of H_2 sensing characteristics performed at the operating temperature of 400 ^oC with different H_2 gas concentrations (0.015–1.0 vol%) and metal loading levels (2.0 mol%). The interaction of the resistive sensors with a target gas resulted in a change in electrical conductance upon the gas exposure. The original baseline in resistance was quite stable after recovering from multiple gas exposures. When a reducing gas was detected using n-type semiconductors (TiO_2), the resistance decreased due to the increased number of electrons on the semiconductor surface. In addition, the resistance change was enhanced significantly with metal loading and was monotonically increased with gas concentration.

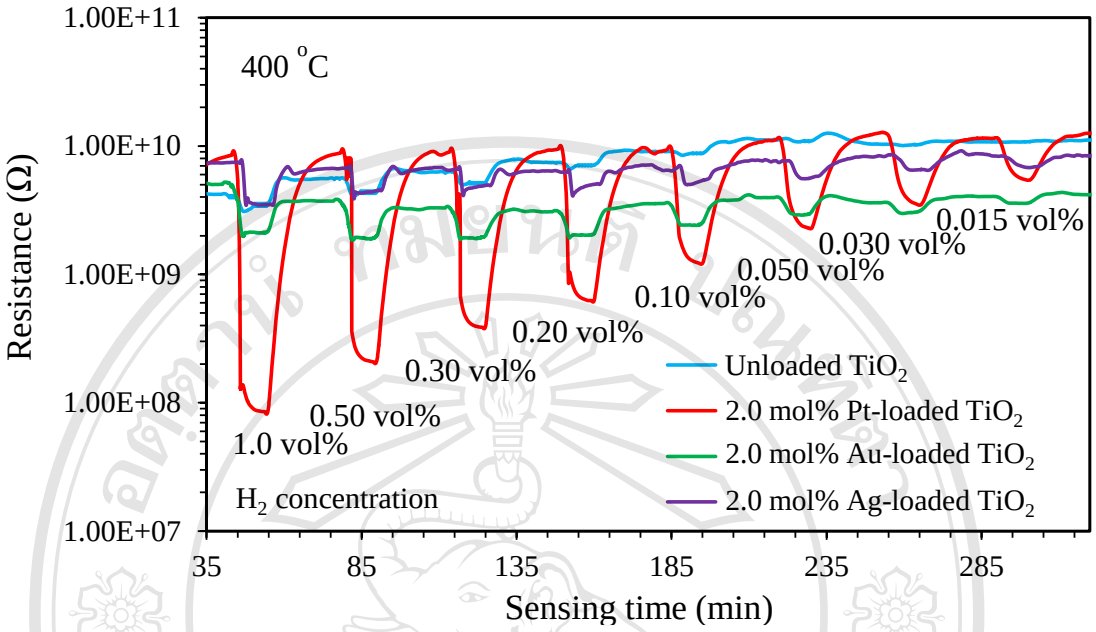

Figure 3.9 The change in resistance of metal-loaded TiO_2 sensors, under exposure to H_2 pulses with varying concentrations from 0.015 to 1.0 vol% 400 °C.

The sensing behaviors were subsequently analyzed in terms of sensor response (S) (left axis) and response time (right axis) (T_{res}) time as illustrated in Figures 3.10. The sensor response greatly increased with increasing Pt loading level up to 2.0 mol% but decreased as the loading level increased further to 3.0 mol% at all gas concentrations (Figure 3.10 (a)). Figures 3.10 (b) and (c) increasing Au and Ag loading level up to 0.75 and 1.0 mol% the sensor response greatly increased but decreased as the loading level of Au and Ag increased further, respectively. It can be seen that, response time decreased of versus increasing H_2 concentration with metal-loaded TiO_2 sensor at operating temperature ranging from 300 °C to 400 °C. In addition, the sensor response increased, indicating that the hydrogen response followed the well-known power law [58, 85].

The recovery time increased relatively slowly with increasing H_2 concentration and was rather insensitive to metal loading level. The recovery time naturally increased with gas concentration due to longer time required to desorb larger amount of adsorbed gas species at high concentration while metal does not play a direct role in desorption of hydrogen. The metal-loaded TiO_2 sensors require rather long recovery time, which could be due to longer time required for gas to diffuse out of the thick and porous TiO_2 layer.

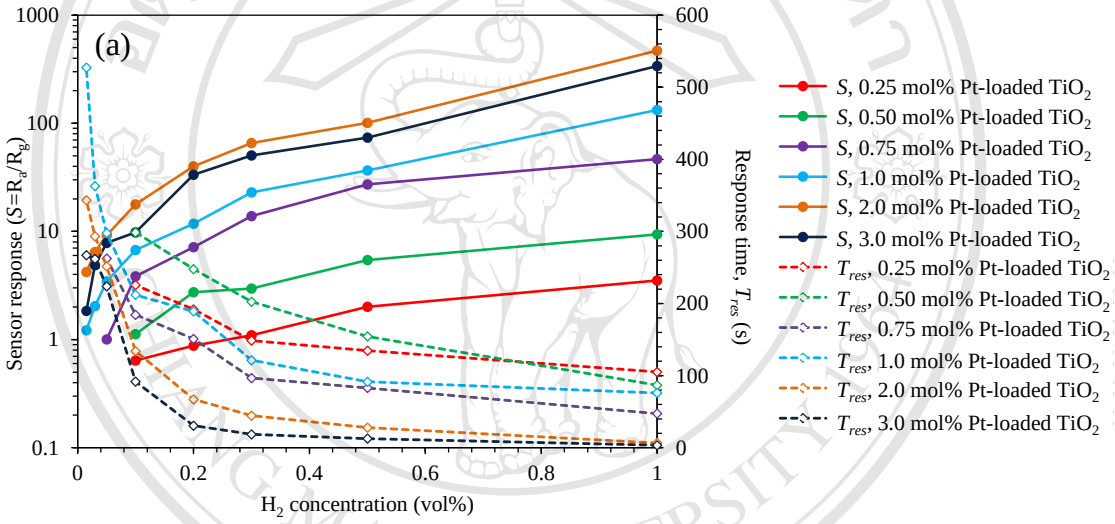

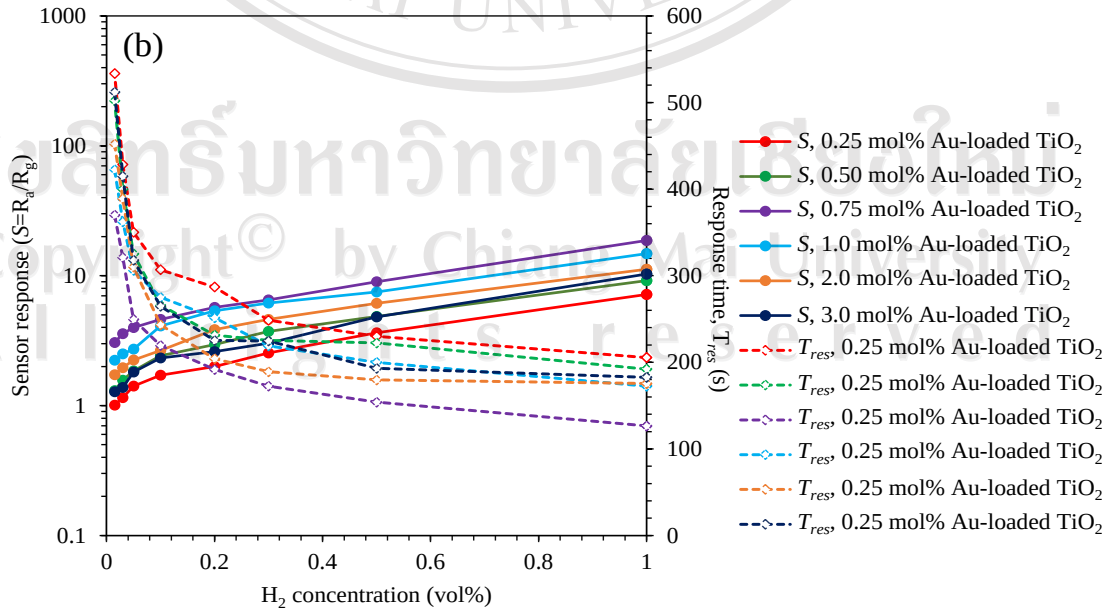

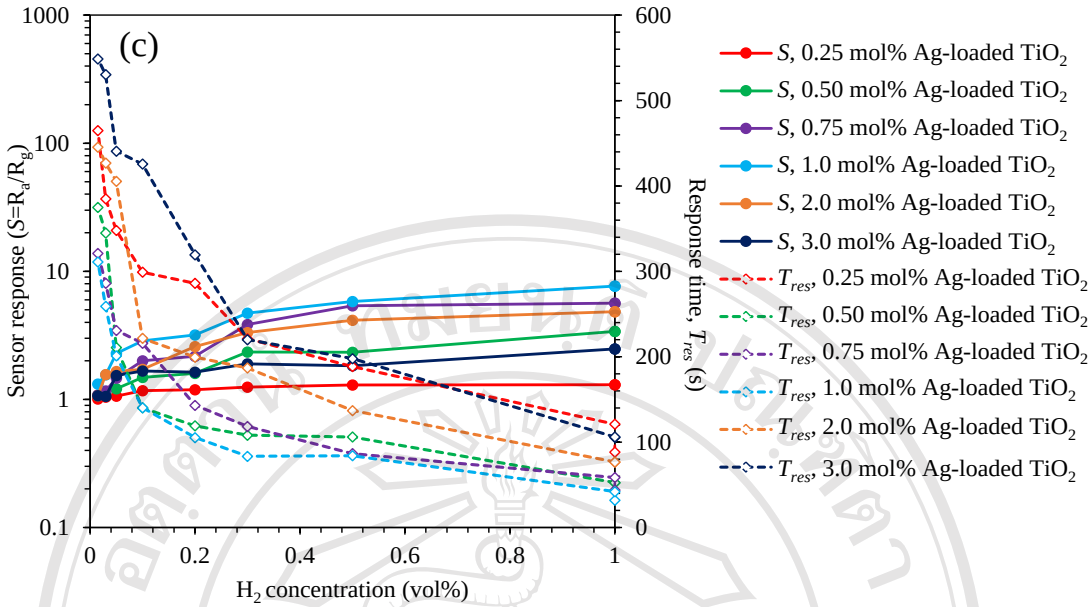

Figure 3.10 The sensor response (S) (left axis) and response time (T_{res}) (right axis) versus H_2 concentration ranging from 0.015–1.0 vol% of 0.25, 0.50, 0.75, 1.0, 2.0 and 3.0 mol% (a) Pt, (b) Au and (c) Ag-loaded TiO_2 sensor at 300 ºC.

Operating temperature generally has an important impact on the performance of semiconductor gas sensors. Typically, the sensing response of the metal oxides tends to increase with increasing temperature [136–137]. Figure 3.11 shows example of the electrical resistance in air of 2.0 mol% Pt-loaded TiO_2 thick-film sensor as a function of time at different temperatures of 300, 350, and 400 ºC for the thick films of 2.0 mol% Pt-loaded TiO_2. It was shown that the baseline resistance of the Pt-loaded sensor tends to decrease with increasing operating temperature while the resistances under 1.0 vol% hydrogen exposure are quite similar. Thus, the resistance change and corresponding response are decreased with increasing operating temperature. The effects of Pt, Au and Ag loading level and operating temperature on gas-sensing response of 1.0 vol% H_2 performed at 300–400 ºC are shown in Figure 3.12. Pt-loaded TiO_2 sensors exhibited

relatively high responses at 300 ºC and the response at the optimal operating temperature was particularly pronounced at 2.0 mol% Pt loading concentration as shown in Figure 3.12 (a). At higher operating temperature (350, 400 ºC), Pt loading provided relatively lower enhancement of sensor response. Thus, the suitable operating temperature and concentration of Pt loading can greatly improve H_2 response of TiO_2 sensors. The best sensing performance with a high sensor response to 1.0 vol% of H_2 concentration of 470 was obtained at the optimal Pt-loading level of 2.0 mol% and optimal operating temperature of 300 ºC. At optimal Au and Ag-loading level of 0.75 and 1.0 mol% of the best sensing performance with a high sensor response to 1.0 vol% of H_2 concentration of 21.6 and 11.9 was obtained at optimal operating temperature of 400 and 350 ºC, respectively (Figure 3.12 (b) and (c)).

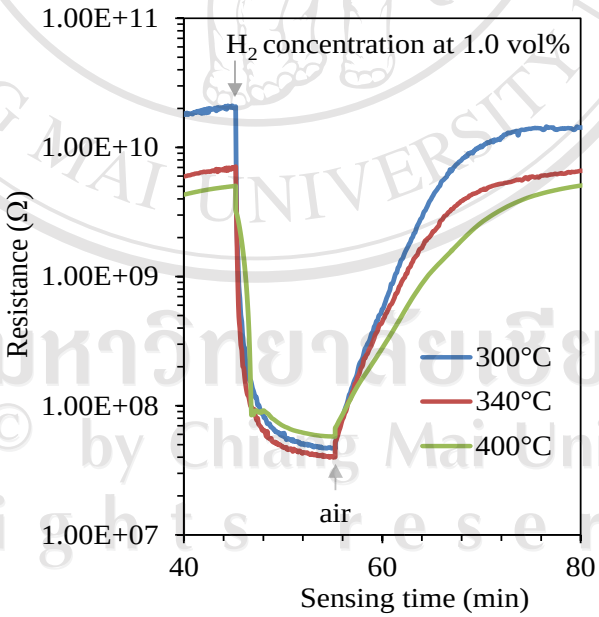

Figure 3.11 Electrical resistance change induced at 300, 350 and 400 ºC for the thick films of 2.0 mol% Pt-loaded TiO_2.

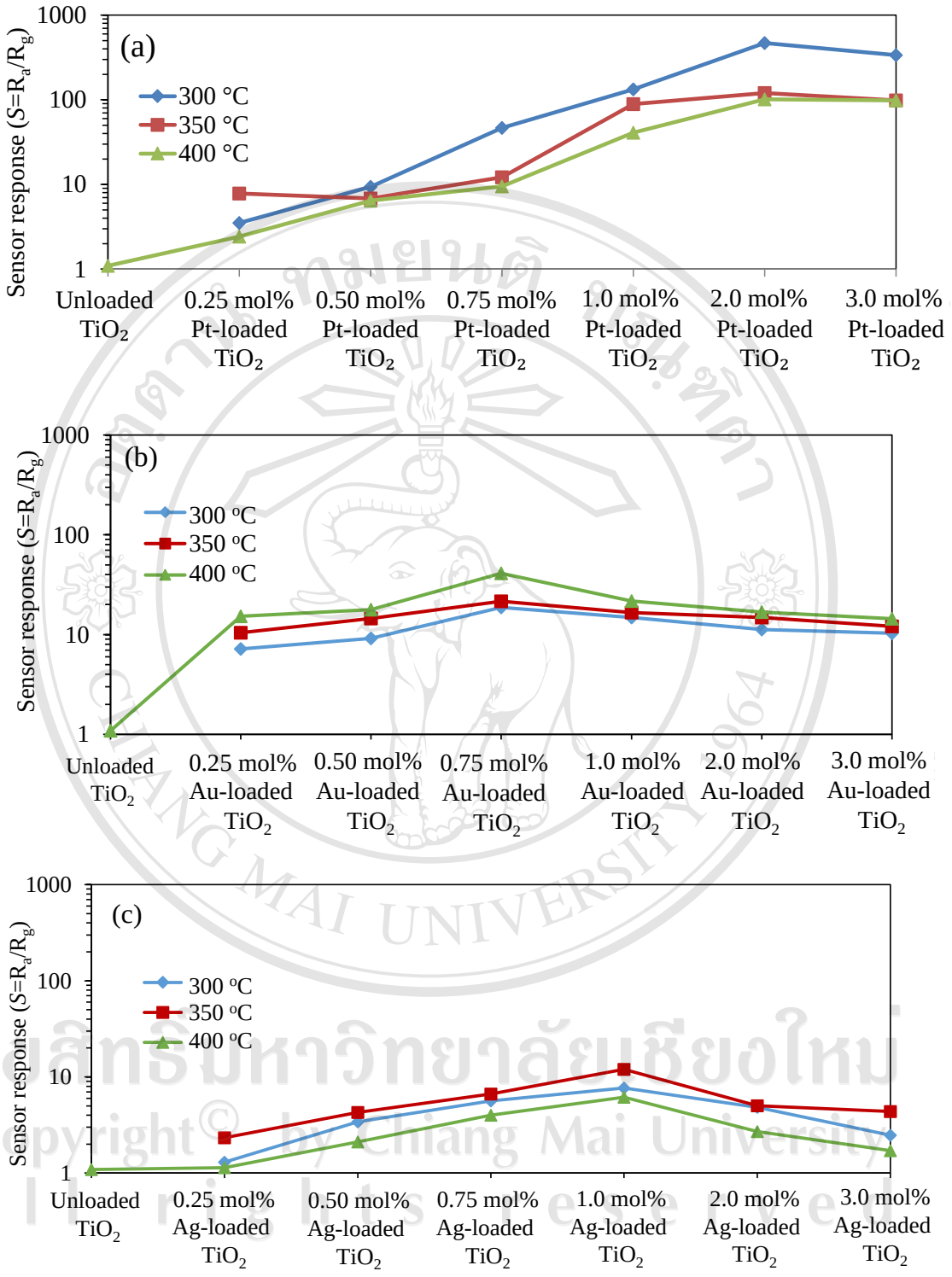

Figure 3.12 Variation of (a) Pt, (b) Au and (c) Ag-loaded TiO_2 sensor response to 1.0 vol% of H_2 with different the operating temperatures ranging from 300–400 °C.

From experimental results, unloaded TiO_2 sensor exhibited very low response to H_2 at operating temperatures 300–400 ^oC, which is in accordance with other reports indicating that direct dissociation of hydrogen on metal oxides will be effective above 400 ^oC [138]. With metal loading in the range between 0.25 and 3.0 mol%, hydrogen response increased substantially. It has been widely accepted that metal enhances sensitivity and response rate of a metal oxide sensor via chemical sensitization with hydrogen gas. Pt can dissociate H_2 into H atoms, which interact with TiO_2 support via the spillover process according to the reaction [139]:

$$H_2 \rightarrow 2H_{(ad)} \tag{3.1}$$

The adsorbed H_2 molecules will interact with the preadsorbed oxygen species including O_2^-, O^-, and O^{2-}, which were thermally activated on Pt-loaded TiO_2 surface, according to [140–143]:

$$4H_{ad} + O^-_{2\,(ad)} \rightarrow 2H_2O_{(des)} + e^- \tag{3.2}$$

$$2H_{ad} + O^-_{(ad)} \rightarrow H_2O_{(des)} + e^- \tag{3.3}$$

$$2H_{ad} + O^{2-}_{(ad)} \rightarrow H_2O_{(des)} + 2e^- \tag{3.4}$$

These reactions produce more electrons and thus increase the conductivity of n-type semiconductor (TiO_2) upon exposure to H_2 with preadsorbed oxygen which leads to freeing of previously trapped electrons.

.

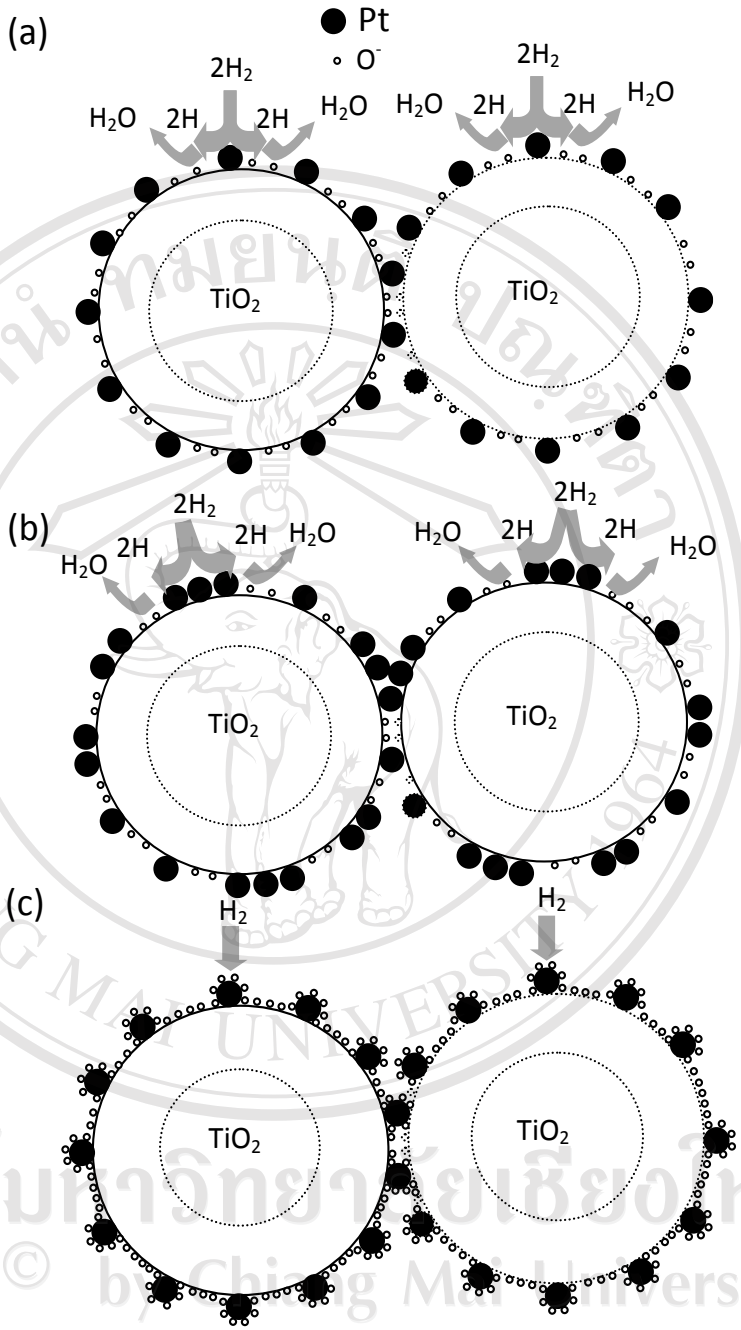

Figure 3.13 Schematic gas sensing mechanisms of Pt-loaded TiO_2 nanoparticles with (a) optimal Pt concentration and (b) excessive Pt concentration at high operating temperature (350–400 ^oC), concentration (3.0 mol%) at low operating temperature (300 ^oC) and (c) with optimal Pt.

In order for the catalyst to be effective, there must be a good dispersion and appropriate amount of the catalysts; thus, catalyst particles are available near most interparticle contacts as illustrated in Figure 3.13 (a). The spillover species must be able to migrate to most interparticle contacts in order to dominate the metal oxide resistance. The spillover mechanism will become less effective when catalyst particles are agglomerated or poorly dispersed as depicted in Figure 3.13 (b). The agglomeration and poor dispersion of Pt nanoparticles reduce the number of spillover hydrogen species on TiO_2 support, thereby reducing the hydrogen response. Such aggregation is highly likely when the Pt loading concentration increases to a level as high as 3.0 mol%. Thus, 2.0, 0.75 and 1.0 mol% is the optimal metal loading level that yields high amount of Pt, Au and Ag with good dispersion on FSP-made TiO_2 nanoparticle supports, which results in an optimal hydrogen response, respectively.

For the effect of operating temperature, Pt, Au and Ag-loaded TiO_2 films exhibited optimum hydrogen response at temperature of 300, 400 and 350 ^oC, respectively and higher operating temperature leads to considerably degraded response. An explanation of sensor response of the temperature-induced change may be formulated by considering the occurrence of different types and concentrations of ionosorbed surface reactive oxygen species (O_2^-, O^-, or O^{2-}) on the metal-loaded TiO_2 surface together with spillover effect [122, 144–149]. At a high temperature (i.e., 350–400 ^oC) (Figure 3.13 (c)), the number of adsorbed oxygen species, particularly O^- or O^{2-}, increased significantly and some of them adsorbed around the metal nanoparticles. The adsorbed oxygen species will shield metal particles from H_2 and reduce ability of H_2 dissociation by metal. Thus, hydrogen response decreases considerably because the spillover effect by metal is substantially hindered while the

rate of direct hydrogen reduction by TiO_2 is still very low. The noble metal on the surface of the metal oxide has the role to enrich its surface or the interface with reactive species such as oxygen ions [150–151]. Therefore, the responsible sensing reaction takes place at the surface of the supporting metal oxide, as shown in Figure 3.13.

3.2.2 Gas sensing of metal-loaded TiO_2 nanoparticles synthesized by FSP towards ethanol gas

Ethanol is a volatile, colorless liquid that has a slight odor with the structural formula C_2H_5OH. In dilute aqueous solution, it has a somewhat sweet flavor, but in more concentrated solution, it has a burning taste. Detection of ethanol vapor is an important feature of the breath alcohol content or even to detect leaks in industrial lines. Ethanol detection is primarily in the range of 10–5000 ppm for monitoring human blood alcohol level and its TLV is 1000 ppm [152]. In addition, ethanol concentration is sometimes measured near its explosive range of 3–19 vol%.

The ethanol gas-sensing properties of unloaded TiO_2 and 0.25–3.0 mol% Au-loaded TiO_2 sensors were tested. It is well known that rate of gas response (The gas-sensing response, S is defined as the ratio R_a/R_g) to C_2H_5OH was much dependent on the operating temperature and the amounts of additives. Such tendencies were shown in Figure 3.14.

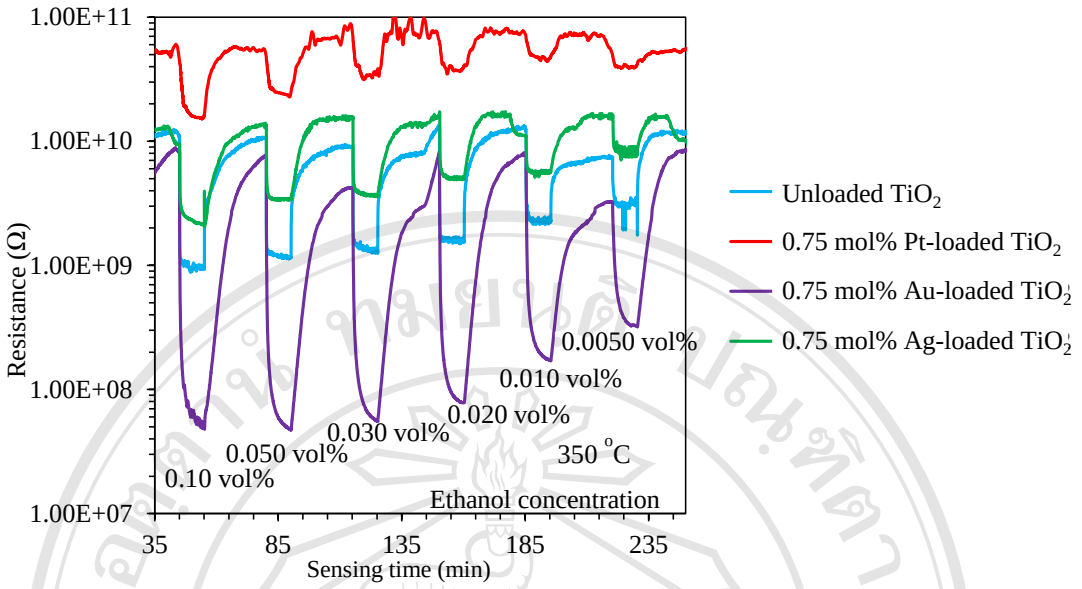

Figure 3.14 The change in resistance of metal-loaded TiO_2 sensors, under exposure to C_2H_5OH pulses with varying concentrations from 0.0050 to 0.10 vol% 350 °C.

Figure 3.14 shows the dynamic response to C_2H_5OH (0.10–0.0050 vol%) of TiO_2 films with difference metal contents at operating temperature of 350 °C. It can be seen that the resistant of all TiO_2 sensors decreased upon the exposure to C_2H_5OH which is a reducing gas, indicating that both the unloaded TiO_2 and metal-loaded TiO_2 films show the typical n-type semiconductor behavior. Comparing to unloaded TiO_2 film, all metal-loaded TiO_2 films had much lower resistance when exposed to C_2H_5OH. In addition, metal-loaded TiO_2 film showed the highest response to C_2H_5OH. These results could be assumed that the gas sensing properties of TiO_2 nanoparticle films could be greatly improved by loading with an appropriate amount of metal.

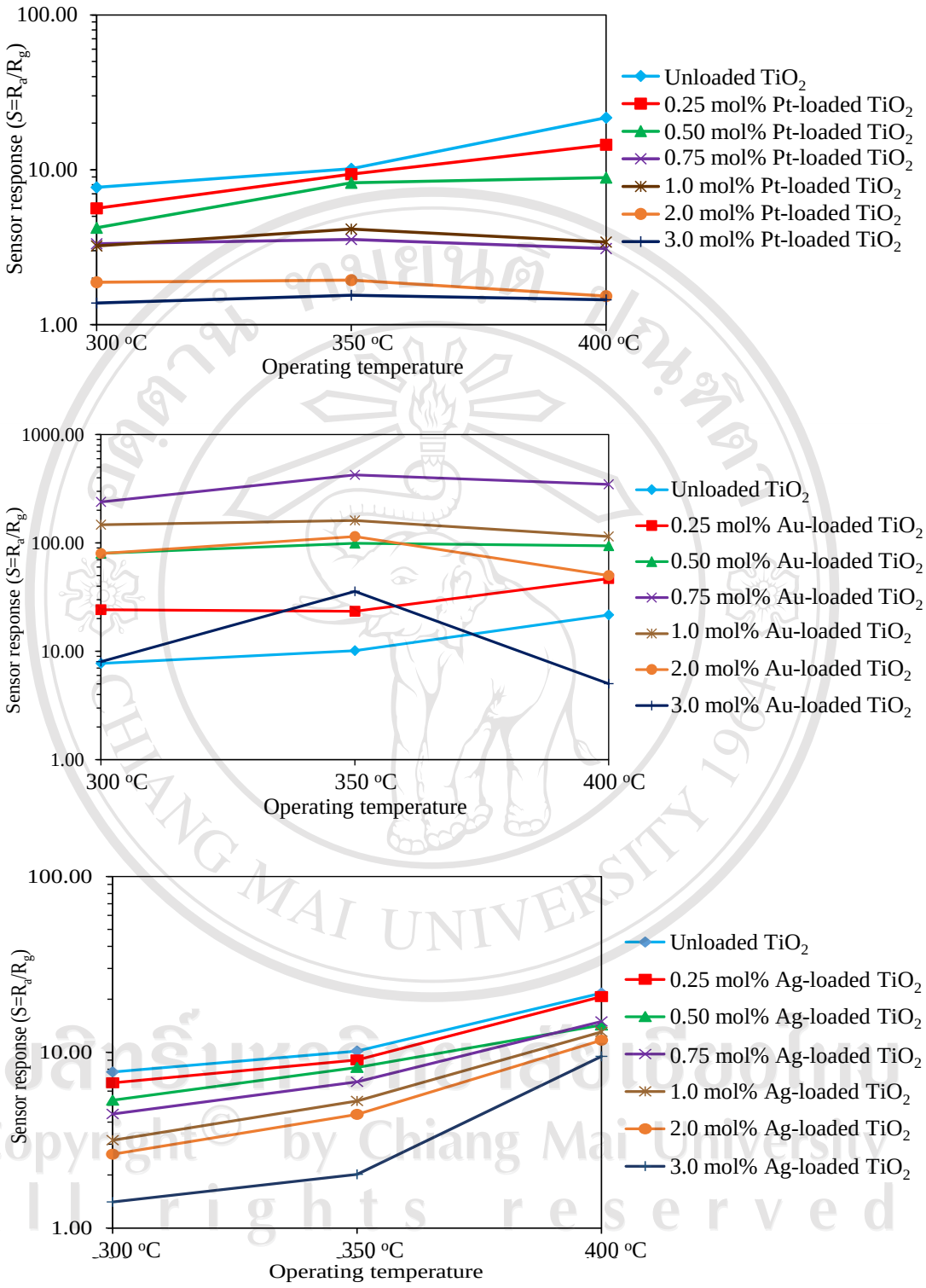

Figure 3.15 Response of unloaded TiO_2, (a) Pt, (b) Au and (c) Ag-loaded TiO_2 sensors operated at 300–400 ºC towards 0.10 vol% C_2H_5OH.

Figure 3.15 demonstrates the sensor response of unloaded and metal-loaded TiO_2 sensors to different concentrations of metals with C_2H_5OH (0.10 vol%) measured at the same operating temperature of 300–400 ^oC. It can be seen that the gas response of the Au loaded sensors is higher than that of the unloaded TiO_2 and the sensor response of Pt and Ag loaded sensors is lower than that of the unloaded TiO_2. In addition, the sensor response values of the sensors increased drastically while response time decreases exponentially with an increase of the C_2H_5OH gas concentration. Thus, it was obviously seen from Figure 3.16 that not only temperature but also ethanol concentration plays a role in determining the response of the sensing films.

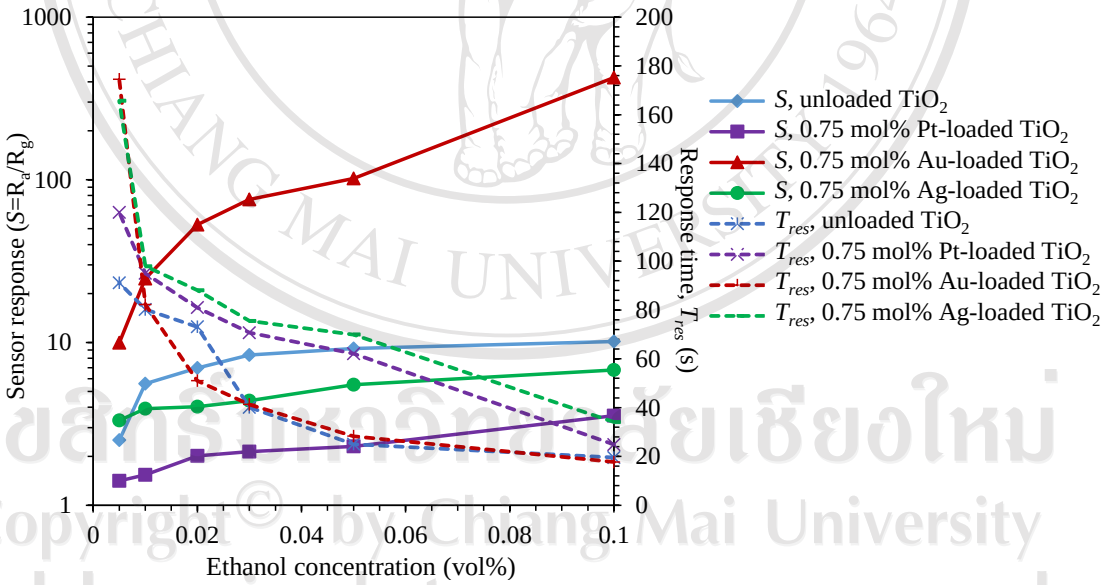

Figure 3.16 Response (left axis) and response time (T_{res}) (right axis) of unloaded TiO_2, 0.75 mol% metal-loaded TiO_2 sensors to different concentration of C_2H_5OH at 350 ^oC.

From experimental results, it was obviously seen that sensor 0.75 mol% Au-loaded TiO_2 showed the highest response value of ~420 at 350 ^oC towards 0.10 vol% ethanol. When compared ethanol response of sensor with the Pt and Ag loaded sensor, at the operating temperature of 300–400 ^oC, unloaded TiO_2 sensors showed higher maximum response than Pt and Ag-loaded TiO_2 (Figure 3.15).

3.2.3 Gas sensing of metal-loaded TiO_2 nanoparticles synthesized by FSP towards acetone gas

Acetone is the organic compound with the formula $(CH_3)_2CO$. It is a colorless, mobile, flammable liquid, and the simplest ketone. Acetone is produced and disposed of in the human body through normal metabolic processes. It is normally present in blood and urine. People with diabetes produce it in larger amounts. Reproductive toxicity tests show that it has low potential to cause reproductive problems. Pregnant women, nursing mothers and children have higher levels of acetone. Ketogenic diets that increase acetone in the body are used to reduce epileptic attacks in infants and children who suffer from recalcitrant refractory epilepsy [153].

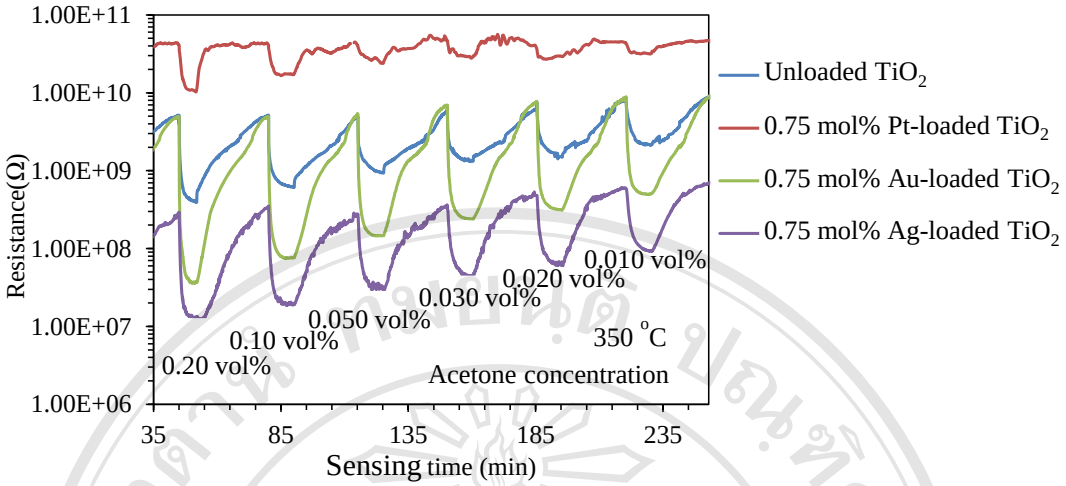

Figure 3.17 The change in resistance of 0.75 mol% Pt, Au and Ag-loaded TiO_2 sensors, under exposure to $(CH_3)_2CO$ pulses with varying concentrations from 0.010 to 0.20 vol%, 350 ^oC.

The effects of Pt, Au and Ag loading level and operating temperature on gas-sensing response of 0.010–0.20 vol% $(CH_3)_2CO$ performed at 350 ^oC are shown in Figure 3.17. It can be seen that the resistant of all TiO_2 sensors decreased upon the exposure to $(CH_3)_2CO$ which is an reducing gas, indicating that both the unloaded TiO_2 and metal-loaded TiO_2 films still behave as n-type semiconductor behavior. Pt-loaded TiO_2 sensors exhibited relatively high responses at 400 ^oC and the response at the optimal operating temperature was particularly pronounced at 0.50 mol% Pt loading concentration as shown in Figure 3.18 (a). Thus, the suitable operating temperature and concentration of Pt loading can greatly improve $(CH_3)_2CO$ response of TiO_2 sensors. The best sensing performance with a high sensor response to 0.20 vol% of $(CH_3)_2CO$ concentration of ~244 was obtained at the optimal Pt-loading level of 0.50 mol% and optimal operating temperature of 300 ^oC. At optimal Au and Ag-loading level of 0.75 mol% of the best sensing performance with a high sensor response to 0.20 vol% of $(CH_3)_2CO$

concentration of ~194 and ~161 was obtained optimal operating temperature of 350 ºC, respectively (Figures 3.18 (b) and (c)).

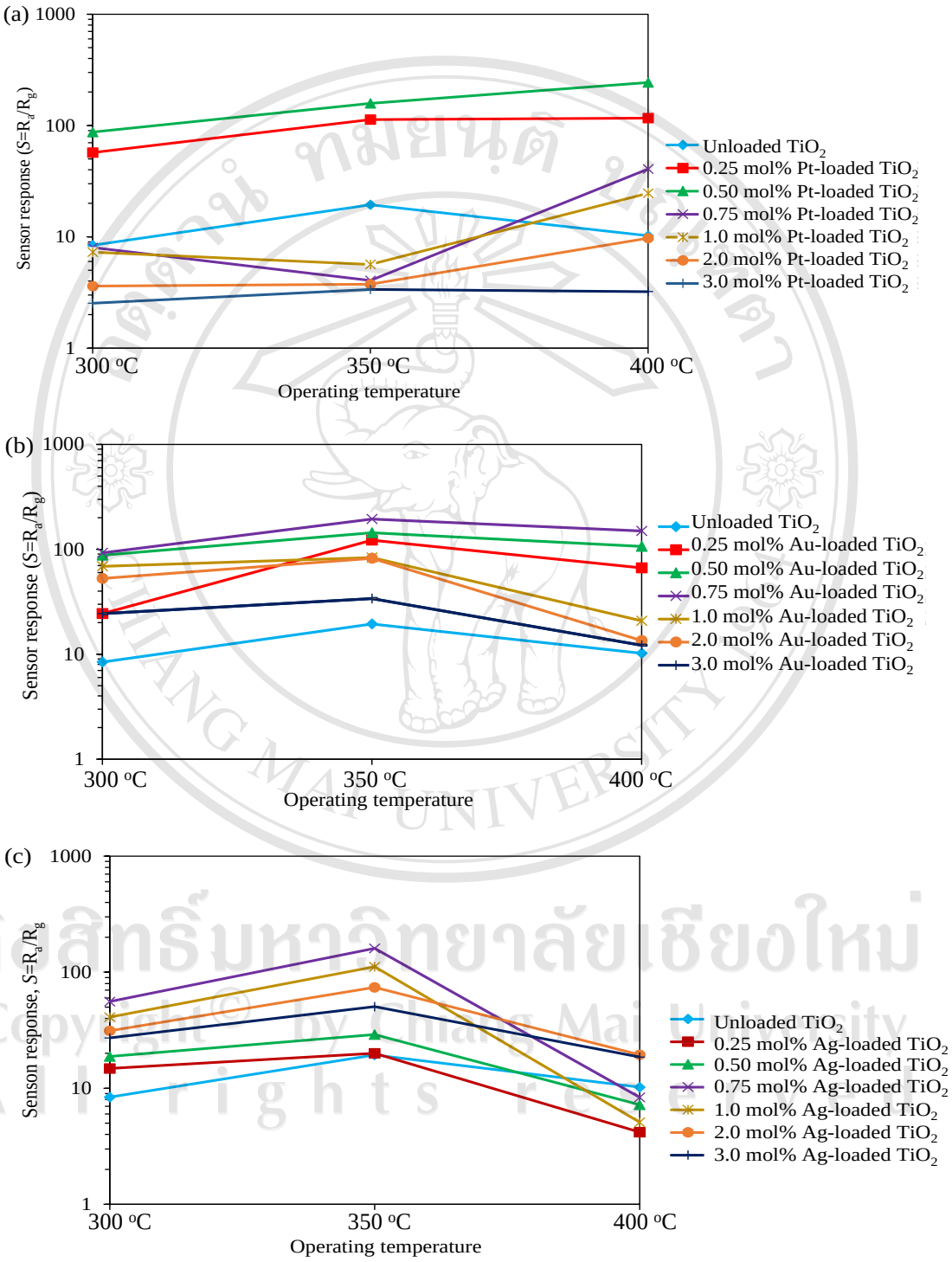

Figure 3.18 Response of unloaded TiO_2, (a) Pt, (b) Au and (c) Ag-loaded TiO_2 sensors operated at 300–400 ºC towards 0.20 vol% $(CH_3)_2CO$.

The response and response time versus the $(CH_3)_2CO$ concentrations ranging from 0.010–0.20 vol% concentration based on TiO_2 nanoparticles at operating temperature of 400 °C are shown in Figure 3.19. It can be seen that the semiconducting and gas sensing behaviors are strongly depending on the metal loading concentrations in TiO_2 nanoparticles. By loading TiO_2 nanoparticles with metal, the $(CH_3)_2CO$ response was increased and response time was reduced. As the Pt loading concentration at 0.50 mol%, the response increases by more than 0.50 mol% of Au and Ag loading.

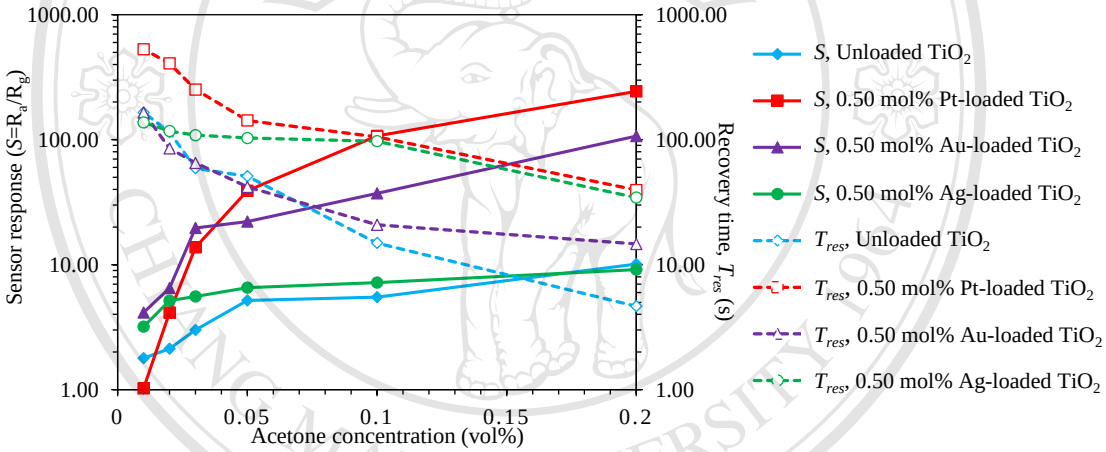

Figure 3.19 Response (left axis) and response time (T_{res}) (right axis) of unloaded TiO_2 and metal-loaded TiO_2 sensors to different concentration of $(CH_3)_2CO$ at 400 °C.

3.2.4 Gas sensing of metal-loaded TiO_2 nanoparticles synthesized by FSP towards carbon monoxide gas

Carbon monoxide (CO) is a colorless and odorless gas, making it undetectable to human [154]. It is mainly produced due to the incomplete combustion of fuels and commonly found in the emission of automobile exhaust. The gas has been shown to

bind irreversibly to the iron center of hemoglobin, the oxygen transport molecule in blood. Thus, oxygen can no longer be absorbed and high levels of CO exposure will result in death. CO is mainly of interest as toxic gases and its detection range of interest is typically 1–1,000 ppm because its TLV is 25 ppm. However, CO is also explosive and there is some interest for its measurement in the high concentration range near its minimum explosive limit of 12.5 vol%.

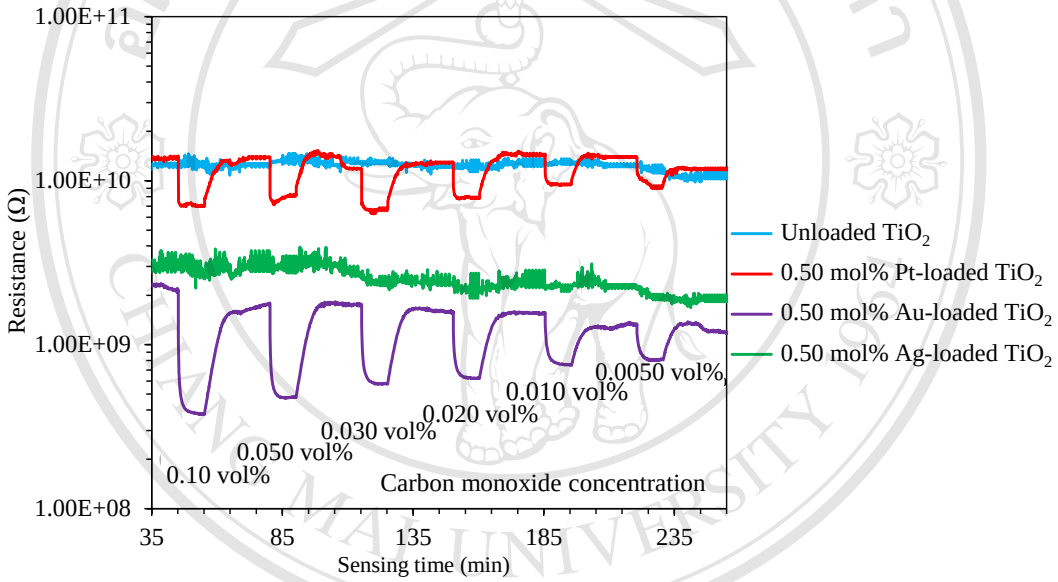

Figure 3.20 The change in resistance of 0.50 mol% Pt, Au and Ag-loaded TiO_2 sensors, under exposure to CO pulses with varying concentrations from 0.0050 to 0.10 vol% 350 ^{o}C.

The dynamic response to CO (0.0050–0.10 vol%) of TiO_2 films with different metal contents at operating temperature of 350 ^{o}C are shown in Figure 3.20. It can be seen that the resistant of all TiO_2 sensors decreased upon the exposure to CO which is a reducing gas, indicating that both the unloaded TiO_2 and metal-loaded TiO_2 films

still behave as n-type semiconductor. The resistances of all metal-loaded TiO_2 films were comparable to unloaded TiO_2 film when exposed to CO at any concentrations. Moreover for the Pt and Au loaded samples, the Pt and Au-loaded TiO_2 film showed the response to this gas. The unloaded TiO_2 and Ag-loaded TiO_2 cannot detect this gas.

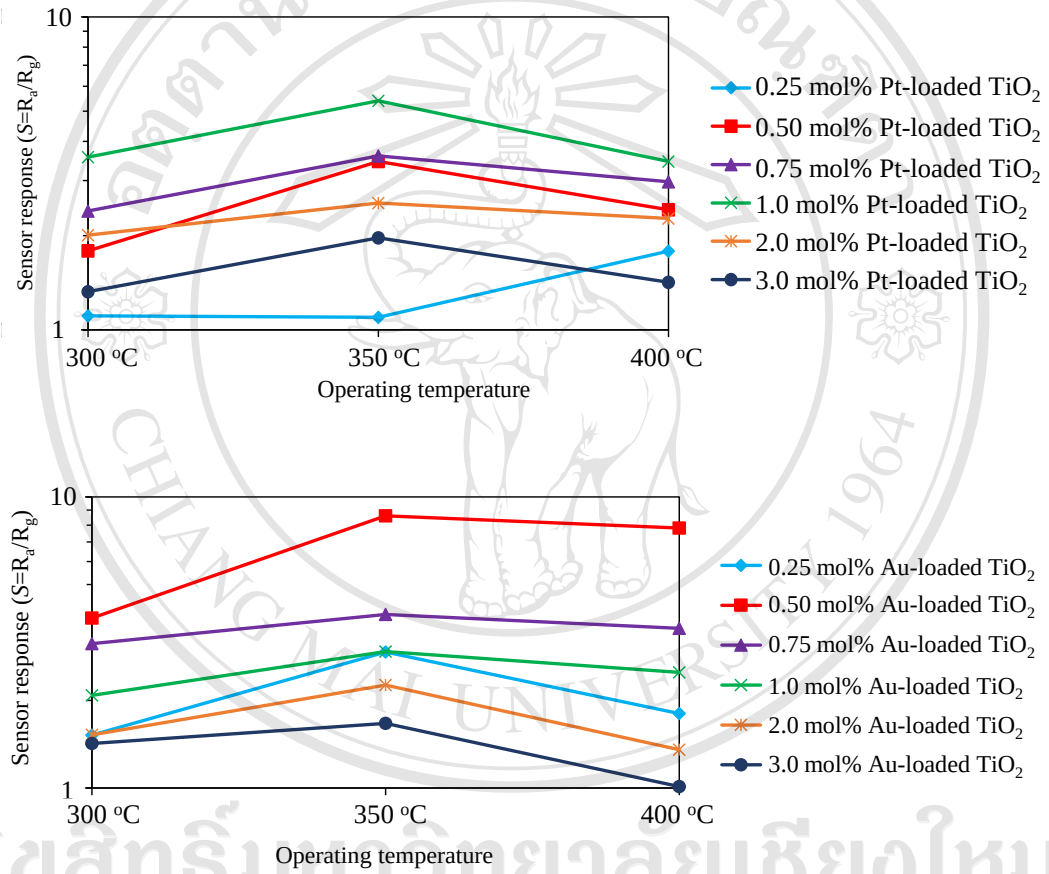

Figure 3.21 Response of (a) Pt and (b) Au-loaded TiO_2 sensors operated at 300–400 ºC towards 0.10 vol% CO.

The temperature has an obvious influence on the response of sensors to CO gas (The gas-sensing response, S is defined as the ratio R_a/R_g). In order to determine the optimal operating temperatures, the response of Pt and Au-loaded TiO_2 sensors

with concentrations to 0.10 vol% of CO in air was tested as a function operating temperature, as shown in Figure 3.21. It can be seen that response of sensor 1.0 mol% Pt-loaded TiO_2 and 0.50 mol% Au-loaded TiO_2 showed high response value of ~5.4 and ~8.6, respectively at CO concentration of 0.10 vol%.

3.2.5 Gas sensing of metal-loaded TiO_2 nanoparticles synthesized by FSP towards sulfur dioxide gas

Sulfur dioxide (SO_2), at standard atmosphere it is a toxic gas with a pungent, irritating and rotten smell. It is released naturally by volcanic activity and is a potent global warming gas. In Earth's atmosphere, it exists in trace amounts of 1 part per billion (ppb) by volume, primarily as a pollutant commonly released by various industrial processes. Since coal and petroleum often contain sulfur compounds, their combustion generates sulfur dioxide unless the sulfur compounds are removed before burning the fuel. Further oxidation of SO_2, usually in the presence of a catalyst such as NO_2, forms H_2SO_4, and thus acid rain. Sulfur dioxide emissions are also a precursor to particulates in the atmosphere. Both of these impacts are cause for concern over the environmental impact of these fuels. The specific person who discovered sulfur dioxide is not known, but it was first used by the Romans in wine making, when they discovered that burning sulfur candles inside empty wine vessels keeps them fresh and free from vinegar smell [155].

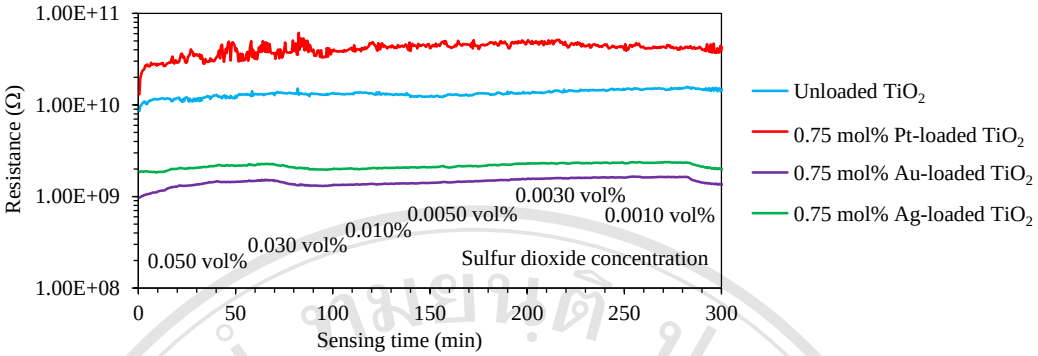

Figure 3.22 The change in resistance of 0.50 mol% Pt, Au and Ag-loaded TiO_2 sensors, under exposure to SO_2 pulses with varying concentrations from 0.0010 to 0.050 vol% 350 ^oC.

The dynamic response to SO_2 (0.0010–0.050 vol%) of TiO_2 films with different metal incorporations at operating temperature of 350 ^oC are shown in Figure 3.22. The resistance of all TiO_2 sensors did not change under exposure to SO_2 which is a reducing gas, indicating that both the unloaded TiO_2 and metal-loaded TiO_2 films still behave as n-type semiconductor. It was found that the sensor response of all unloaded TiO_2 and metal-loaded TiO_2 films could not respond to film when exposed to SO_2 at 300–400 ^oC.

3.2.6 Selective gas sensors based on flame-spray-made metal-loaded TiO_2 nanoparticles

To quantitatively determine the selectivity of sensors, the responses towards H_2, C_2H_5OH, $(CH_3)_2CO$, CO and SO_2 of all sensors were calculated and plotted at the fixed concentration of 0.10 vol% and operating temperature of 350 ^oC as shown in Figure 3.22.

It can be noticed that the sensitivities of all metal-loaded TiO_2 films toward H_2, C_2H_5OH, $(CH_3)_2CO$, CO and SO_2 were clearly improved comparing to unloaded TiO_2.

Figure 3.22 (a) shows that sensor, Pt-loaded TiO_2, exhibits very high $(CH_3)_2CO$ response but much weaker responses to H_2, C_2H_5OH, $(CH_3)_2CO$, CO and SO_2, respectively. The response of 0.50, 1.0 and 2.0 mol% Pt-loaded TiO_2 sensing films towards $(CH_3)_2CO$, H_2 and CO were ~117, 11.6 and 3.39 at 0.10 vol% concentration at 350 ^oC, respectively. As the Pt loading concentration increases from 0 to 3.0 mol%, the response decreases upon the loading to Pt which is a C_2H_5OH gas and no response to SO_2.

The comparison of sensitivity of Au-loaded TiO_2 with different Au concentrations towards 0.10 vol% of $(CH_3)_2CO$, CO, H_2, C_2H_5OH and SO_2 is shown in Figure 3.22 (b). It can be noticed that the sensitivities of all Au-loaded TiO_2 films towards $(CH_3)_2CO$, CO, H_2 and C_2H_5OH were clearly improved comparing to unloaded TiO_2. The sensitivities of all TiO_2 films towards C_2H_5OH were greatly higher than that towards $(CH_3)_2CO$, CO, H_2 and SO_2. The response of 0.75 mol% Au-loaded TiO_2 sensing films towards $(CH_3)_2CO$, H_2 and C_2H_5OH were ~64, 6.0 and 425 at 0.10 vol% concentration at 350 ^oC, respectively. The response of 0.50 mol% Au-loaded TiO_2 sensing films towards CO was ~4.0 at 0.10 vol% concentration at 350 ^oC, As the Au loading concentration increases from 0 to 3.0 mol%, no response upon the loading to Au which is a SO_2 gas.

From Figure 3.22 (c), 0.75 mol% Ag-loaded TiO_2 gas sensor has good gas selectivity to 0.10 vol% of $(CH_3)_2CO$ concentration of 96 at 350 ^oC. The response of 1.0 mol% Ag-loaded TiO_2 sensing films towards hydrogen was 2.9 at 0.10 vol% concentration at 350 ^oC. As the Ag loading concentration increases from 0 to 3.0 mol%, the response decreases upon the loading to Ag which is a C_2H_5OH gas and no response with CO and SO_2 gas.

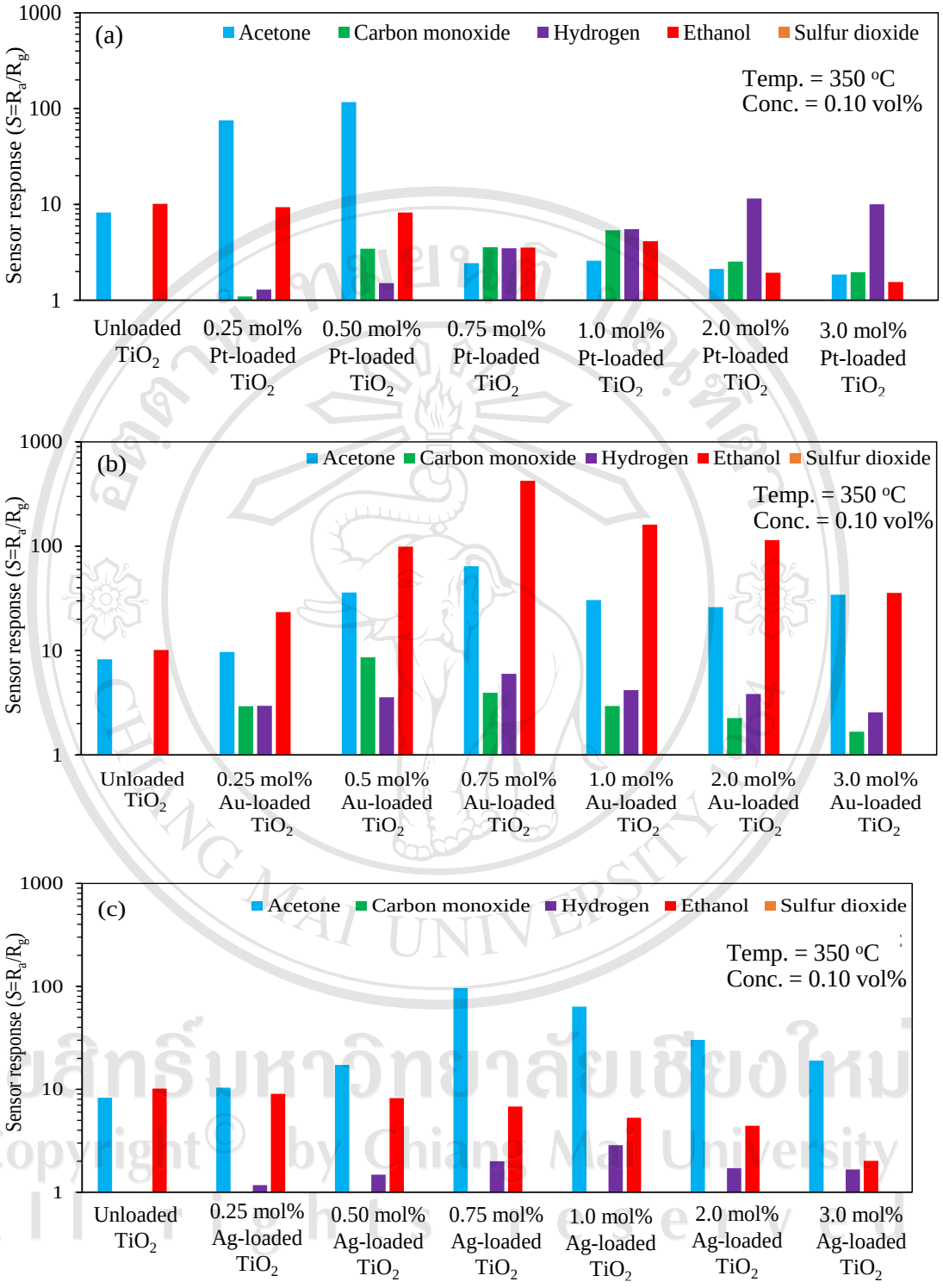

Figure 3.22 The selectivity histograms of (a) Pt, (b) Au and (c) Ag-loaded TiO_2 sensors for explosive gases at concentration of 0.10 vol% and operating temperature of 350 °C.

3.3 Summary of characteristics of unloaded TiO_2 and metal-loaded TiO_2 nanoparticles synthesized by FSP

Tables 3.1 shows the summary of characteristics of unloaded TiO_2 and metal-loaded TiO_2 nanoparticles synthesized by FSP method.

Table 3.1 Summary of characteristics of unloaded TiO_2 and Pt-loaded TiO_2 nanoparticles synthesized by FSP

Material characterization methods	**Unloaded TiO_2 and metal-loaded TiO_2 nanoparticles**
XRD	TiO_2, Anatase (tetragonal), JCPDS No. 21–1272 TiO_2, Rutile (tetragonal) JCPDS No. 21–1276 Platinum (cubic face centered) JCPDS No. 87–0640 Gold (cubic face centered) JCPDS No. 04–0784 Silver (cubic face centered) JCPDS No. 87–0717
BET	Size : ~9−10 nm of unloaded TiO_2 Size : ~14−38 nm of Pt-loaded TiO_2 Size : ~14−27 nm of Au-loaded TiO_2 Size : ~14−24 nm of Ag-loaded TiO_2
TEM	Size : ~9−25 nm of unloaded TiO_2 Size : ~10−50 nm of Pt-loaded TiO_2 Size : ~10−60 nm of Au-loaded TiO_2 Size : ~10−80 nm of Ag-loaded TiO_2

Tables 3.2 show the summary of gas sensing performances of unloaded TiO_2 sensor synthesized by FSP method.

Table 3.2 Summary of gas sensing performances of unloaded TiO_2 and metal-loaded TiO_2 sensor synthesized by FSP

Materials	**Gas concentration**	**Temp.**	**Response ($S=R_a/R_g$)**
Unloaded TiO_2	H_2 (1.0 vol%)	300 °C	No response
		350 °C	No response
		400 °C	~2.37
Unloaded TiO_2	$(CH_3)_2CO$ (0.20 vol%)	300 °C	~8.40
		350 °C	~19.4
		400 °C	~10.1
Unloaded TiO_2	CO (0.10 vol%)	300 °C	No response
		350 °C	No response
		400 °C	No response
Unloaded TiO_2	C_2H_5OH (0.10 vol%)	300 °C	~7.72
		350 °C	~10.2
		400 °C	~21.7
Unloaded TiO_2	SO_2 (0.050 vol%)	300 °C	No response
		350 °C	No response
		400 °C	No response

Table 3.2 (Cont.) Summary of gas sensing performances of unloaded TiO_2 and metal-loaded TiO_2 sensor synthesized by FSP

Materials	**Gas concentration**	**Temp.**	**Response ($S=R_a/R_g$)**
0.25 mol% Pt-loaded TiO_2	H_2 (1.0 vol%)	300 °C	~3.51
		350 °C	~2.64
		400 °C	~3.58
0.25 mol% Pt-loaded TiO_2	$(CH_3)_2CO$ (0.20 vol%)	300 °C	~57.0
		350 °C	~113
		400 °C	~117
0.25 mol% Pt-loaded TiO_2	CO (0.10 vol%)	300 °C	~1.17
		350 °C	~1.10
		400 °C	~1.79
0.25 mol% Pt-loaded TiO_2	C_2H_5OH (0.10 vol%)	300 °C	~5.64
		350 °C	~9.38
		400 °C	~14.5
0.25 mol% Pt-loaded TiO_2	SO_2 (0.050 vol%)	300 °C	No response
		350 °C	No response
		400 °C	No response

Table 3.2 (Cont.) Summary of gas sensing performances of unloaded TiO_2 and metal-loaded TiO_2 sensor synthesized by FSP

Materials	**Gas concentration**	**Temp.**	**Response ($S=R_a/R_g$)**
0.50 mol% Pt-loaded TiO_2	H_2 (1.0 vol%)	300 °C	~9.38
		350 °C	~6.82
		400 °C	~6.45
0.50 mol% Pt-loaded TiO_2	$(CH_3)_2CO$ (0.20 vol%)	300 °C	~87.3
		350 °C	~158
		400 °C	~244
0.50 mol% Pt-loaded TiO_2	CO (0.10 vol%)	300 °C	~1.79
		350 °C	~3.46
		400 °C	~2.42
0.50 mol% Pt-loaded TiO_2	C_2H_5OH (0.10 vol%)	300 °C	~4.22
		350 °C	~8.24
		400 °C	~8.89
0.50 mol% Pt-loaded TiO_2	SO_2 (0.050 vol%)	300 °C	No response
		350 °C	No response
		400 °C	No response

Table 3.2 (Cont.) Summary of gas sensing performances of unloaded TiO_2 and metal-loaded TiO_2 sensor synthesized by FSP

Materials	**Gas concentration**	**Temp.**	**Response ($S=R_a/R_g$)**
0.75 mol% Pt-loaded TiO_2	H_2 (1.0 vol%)	300 °C	~46.7
		350 °C	~12.2
		400 °C	~9.50
0.75 mol% Pt-loaded TiO_2	$(CH_3)_2CO$ (0.20 vol%)	300 °C	~8.02
		350 °C	~4.05
		400 °C	~40.7
0.75 mol% Pt-loaded TiO_2	CO (0.10 vol%)	300 °C	~2.40
		350 °C	~3.59
		400 °C	~2.97
0.75 mol% Pt-loaded TiO_2	C_2H_5OH (0.10 vol%)	300 °C	~3.33
		350 °C	~3.55
		400 °C	~3.10
0.75 mol% Pt-loaded TiO_2	SO_2 (0.050 vol%)	300 °C	No response
		350 °C	No response
		400 °C	No response

Table 3.2 (Cont.) Summary of gas sensing performances of unloaded TiO_2 and metal-loaded TiO_2 sensor synthesized by FSP

Materials	**Gas concentration**	**Temp.**	**Response ($S=R_a/R_g$)**
1.0 mol% Pt-loaded TiO_2	H_2 (1.0 vol%)	300 °C	~133
		350 °C	~89.2
		400 °C	~41.0
1.0 mol% Pt-loaded TiO_2	$(CH_3)_2CO$ (0.20 vol%)	300 °C	~7.28
		350 °C	~5.64
		400 °C	~24.7
1.0 mol% Pt-loaded TiO_2	CO (0.10 vol%)	300 °C	~3.57
		350 °C	~5.39
		400 °C	~3.46
1.0 mol% Pt-loaded TiO_2	C_2H_5OH (0.10 vol%)	300 °C	~3.22
		350 °C	~4.14
		400 °C	~3.42
1.0 mol% Pt-loaded TiO_2	SO_2 (0.050 vol%)	300 °C	No response
		350 °C	No response
		400 °C	No response

Table 3.2 (Cont.) Summary of gas sensing performances of unloaded TiO_2 and metal-loaded TiO_2 sensor synthesized by FSP

Materials	**Gas concentration**	**Temp.**	**Response ($S=R_a/R_g$)**
2.0 mol% Pt-loaded TiO_2	H_2 (1.0 vol%)	300 °C	~470
		350 °C	~121
		400 °C	~101
2.0 mol% Pt-loaded TiO_2	$(CH_3)_2CO$ (0.20 vol%)	300 °C	~3.61
		350 °C	~3.75
		400 °C	~9.72
2.0 mol% Pt-loaded TiO_2	CO (0.10 vol%)	300 °C	~2.01
		350 °C	~2.54
		400 °C	~2.27
2.0 mol% Pt-loaded TiO_2	C_2H_5OH (0.10 vol%)	300 °C	~1.88
		350 °C	~1.94
		400 °C	~1.53
2.0 mol% Pt-loaded TiO_2	SO_2 (0.050 vol%)	300 °C	No response
		350 °C	No response
		400 °C	No response

Table 3.2 (Cont.) Summary of gas sensing performances of unloaded TiO_2 and metal-loaded TiO_2 sensor synthesized by FSP

Materials	**Gas concentration**	**Temp.**	**Response ($S=R_a/R_g$)**
3.0 mol% Pt-loaded TiO_2	H_2 (1.0 vol%)	300 °C	~337
		350 °C	~98.2
		400 °C	~98.4
3.0 mol% Pt-loaded TiO_2	$(CH_3)_2CO$ (0.20 vol%)	300 °C	~2.53
		350 °C	~3.36
		400 °C	~3.22
3.0 mol% Pt-loaded TiO_2	CO (0.10 vol%)	300 °C	~1.32
		350 °C	~1.97
		400 °C	~1.42
3.0 mol% Pt-loaded TiO_2	C_2H_5OH (0.10 vol%)	300 °C	~1.38
		350 °C	~1.55
		400 °C	~1.45
3.0 mol% Pt-loaded TiO_2	SO_2 (0.050 vol%)	300 °C	No response
		350 °C	No response
		400 °C	No response

Table 3.2 (Cont.) Summary of gas sensing performances of unloaded TiO_2 and metal-loaded TiO_2 sensor synthesized by FSP

Materials	**Gas concentration**	**Temp.**	**Response ($S=R_a/R_g$)**
0.25 mol% Au-loaded TiO_2	H_2 (1.0 vol%)	300 °C	~7.17
		350 °C	~10.5
		400 °C	~15.2
0.25 mol% Au-loaded TiO_2	$(CH_3)_2CO$ (0.20 vol%)	300 °C	~24.3
		350 °C	~144
		400 °C	~150
0.25 mol% Au-loaded TiO_2	CO (0.10 vol%)	300 °C	~1.52
		350 °C	~2.93
		400 °C	~1.80
0.25 mol% Au-loaded TiO_2	C_2H_5OH (0.10 vol%)	300 °C	~24.2
		350 °C	~23.4
		400 °C	~46.9
0.25 mol% Au-loaded TiO_2	SO_2 (0.050 vol%)	300 °C	No response
		350 °C	No response
		400 °C	No response

Table 3.2 (Cont.) Summary of gas sensing performances of unloaded TiO_2 and metal-loaded TiO_2 sensor synthesized by FSP

Materials	**Gas concentration**	**Temp.**	**Response ($S=R_a/R_g$)**
0.50 mol% Au-loaded TiO_2	H_2 (1.0 vol%)	300 °C	~9.17
		350 °C	~14.5
		400 °C	~17.8
0.50 mol% Au-loaded TiO_2	$(CH_3)_2CO$ (0.20 vol%)	300 °C	~52.8
		350 °C	~122
		400 °C	~107
0.50 mol% Au-loaded TiO_2	CO (0.10 vol%)	300 °C	~3.83
		350 °C	~8.60
		400 °C	~7.81
0.50 mol% Au-loaded TiO_2	C_2H_5OH (0.10 vol%)	300 °C	~80.3
		350 °C	~99.2
		400 °C	~94.2
0.50 mol% Au-loaded TiO_2	SO_2 (0.050 vol%)	300 °C	No response
		350 °C	No response
		400 °C	No response

Table 3.2 (Cont.) Summary of gas sensing performances of unloaded TiO_2 and metal-loaded TiO_2 sensor synthesized by FSP

Materials	**Gas concentration**	**Temp.**	**Response ($S=R_a/R_g$)**
0.75 mol% Au-loaded TiO_2	H_2 (1.0 vol%)	300 °C	~18.7
		350 °C	~21.5
		400 °C	~41.2
0.75 mol% Au-loaded TiO_2	$(CH_3)_2CO$ (0.20 vol%)	300 °C	~68.9
		350 °C	~194
		400 °C	~66.6
0.75 mol% Au-loaded TiO_2	CO (0.10 vol%)	300 °C	~3.13
		350 °C	~3.95
		400 °C	~3.53
0.75 mol% Au-loaded TiO_2	C_2H_5OH (0.10 vol%)	300 °C	~239
		350 °C	~425
		400 °C	~347
0.75 mol% Au-loaded TiO_2	SO_2 (0.050 vol%)	300 °C	No response
		350 °C	No response
		400 °C	No response

Table 3.2 (Cont.) Summary of gas sensing performances of unloaded TiO_2 and metal-loaded TiO_2 sensor synthesized by FSP

Materials	**Gas concentration**	**Temp.**	**Response ($S=R_a/R_g$)**
1.0 mol% Au-loaded TiO_2	H_2 (1.0 vol%)	300 °C	~14.8
		350 °C	~16.6
		400 °C	~21.6
1.0 mol% Au-loaded TiO_2	$(CH_3)_2CO$ (0.20 vol%)	300 °C	~88.0
		350 °C	~83.3
		400 °C	~20.8
1.0 mol% Au-loaded TiO_2	CO (0.10 vol%)	300 °C	~2.08
		350 °C	~2.94
		400 °C	~2.50
1.0 mol% Au-loaded TiO_2	C_2H_5OH (0.10 vol%)	300 °C	~147
		350 °C	~161
		400 °C	~115
1.0 mol% Au-loaded TiO_2	SO_2 (0.050 vol%)	300 °C	No response
		350 °C	No response
		400 °C	No response

Table 3.2 (Cont.) Summary of gas sensing performances of unloaded TiO_2 and metal-loaded TiO_2 sensor synthesized by FSP

Materials	**Gas concentration**	**Temp.**	**Response ($S=R_a/R_g$)**
2.0 mol% Au-loaded TiO_2	H_2 (1.0 vol%)	300 ºC	~11.2
		350 ºC	~14.8
		400 ºC	~16.8
2.0 mol% Au-loaded TiO_2	$(CH_3)_2CO$ (0.20 vol%)	300 ºC	~92.6
		350 ºC	~82.2
		400 ºC	~13.5
2.0 mol% Au-loaded TiO_2	CO (0.10 vol%)	300 ºC	~1.52
		350 ºC	~2.26
		400 ºC	~1.35
2.0 mol% Au-loaded TiO_2	C_2H_5OH (0.10 vol%)	300 ºC	~80.0
		350 ºC	~114
		400 ºC	~50.0
2.0 mol% Au-loaded TiO_2	SO_2 (0.050 vol%)	300 ºC	No response
		350 ºC	No response
		400 ºC	No response

Table 3.2 (Cont.) Summary of gas sensing performances of unloaded TiO_2 and metal-loaded TiO_2 sensor synthesized by FSP

Materials	**Gas concentration**	**Temp.**	**Response ($S=R_a/R_g$)**
3.0 mol% Au-loaded TiO_2	H_2 (1.0 vol%)	300 ºC	~10.3
		350 ºC	~12.1
		400 ºC	~14.4
3.0 mol% Au-loaded TiO_2	$(CH_3)_2CO$ (0.20 vol%)	300 ºC	~24.4
		350 ºC	~33.9
		400 ºC	~12.2
3.0 mol% Au-loaded TiO_2	CO (0.10 vol%)	300 ºC	~1.42
		350 ºC	~1.67
		400 ºC	~1.01
3.0 mol% Au-loaded TiO_2	C_2H_5OH (0.10 vol%)	300 ºC	~8.03
		350 ºC	~35.7
		400 ºC	~5.03
3.0 mol% Au-loaded TiO_2	SO_2 (0.050 vol%)	300 ºC	No response
		350 ºC	No response
		400 ºC	No response

Table 3.2 (Cont.) Summary of gas sensing performances of unloaded TiO_2 and metal-loaded TiO_2 sensor synthesized by FSP

Materials	**Gas concentration**	**Temp.**	**Response ($S=R_a/R_g$)**
0.25 mol% Ag-loaded TiO_2	H_2 (1.0 vol%)	300 °C	~1.30
		350 °C	~2.33
		400 °C	~1.14
0.25 mol% Ag-loaded TiO_2	$(CH_3)_2CO$ (0.20 vol%)	300 °C	~14.8
		350 °C	~20.0
		400 °C	~4.19
0.25 mol% Ag-loaded TiO_2	CO (0.10 vol%)	300 °C	No response
		350 °C	No response
		400 °C	No response
0.25 mol% Ag-loaded TiO_2	C_2H_5OH (0.10 vol%)	300 °C	~6.69
		350 °C	~9.04
		400 °C	~20.7
0.25 mol% Ag-loaded TiO_2	SO_2 (0.050 vol%)	300 °C	No response
		350 °C	No response
		400 °C	No response

Table 3.2 (Cont.) Summary of gas sensing performances of unloaded TiO_2 and metal-loaded TiO_2 sensor synthesized by FSP

Materials	**Gas concentration**	**Temp.**	**Response ($S=R_a/R_g$)**
0.50 mol% Ag-loaded TiO_2	H_2 (1.0 vol%)	300 ºC	~3.40
		350 ºC	~4.27
		400 ºC	~2.11
0.50 mol% Ag-loaded TiO_2	$(CH_3)_2CO$ (0.20 vol%)	300 ºC	~18.8
		350 ºC	~29.1
		400 ºC	~7.20
0.50 mol% Ag-loaded TiO_2	CO (0.10 vol%)	300 ºC	No response
		350 ºC	No response
		400 ºC	No response
0.50 mol% Ag-loaded TiO_2	C_2H_5OH (0.10 vol%)	300 ºC	~5.34
		350 ºC	~8.19
		400 ºC	~14.3
0.50 mol% Ag-loaded TiO_2	SO_2 (0.050 vol%)	300 ºC	No response
		350 ºC	No response
		400 ºC	No response

Table 3.2 (Cont.) Summary of gas sensing performances of unloaded TiO_2 and metal-loaded TiO_2 sensor synthesized by FSP

Materials	**Gas concentration**	**Temp.**	**Response ($S=R_a/R_g$)**
0.75 mol% Ag-loaded TiO_2	H_2 (1.0 vol%)	300 ºC	~5.64
		350 ºC	~6.65
		400 ºC	~4.01
0.75 mol% Ag-loaded TiO_2	$(CH_3)_2CO$ (0.20 vol%)	300 ºC	~55.9
		350 ºC	~161
		400 ºC	~8.36
0.75 mol% Ag-loaded TiO_2	CO (0.10 vol%)	300 ºC	No response
		350 ºC	No response
		400 ºC	No response
0.75 mol% Ag-loaded TiO_2	C_2H_5OH (0.10 vol%)	300 ºC	~4.45
		350 ºC	~6.79
		400 ºC	~15.0
0.75 mol% Ag-loaded TiO_2	SO_2 (0.050 vol%)	300 ºC	No response
		350 ºC	No response
		400 ºC	No response

Table 3.2 (Cont.) Summary of gas sensing performances of unloaded TiO_2 and metal-loaded TiO_2 sensor synthesized by FSP

Materials	**Gas concentration**	**Temp.**	**Response ($S=R_a/R_g$)**
1.0 mol% Ag-loaded TiO_2	H_2 (1.0 vol%)	300 ºC	~7.66
		350 ºC	~12.0
		400 ºC	~6.17
1.0 mol% Ag-loaded TiO_2	$(CH_3)_2CO$ (0.20 vol%)	300 ºC	~41.0
		350 ºC	~112
		400 ºC	~5.11
1.0 mol% Au-loaded TiO_2	CO (0.10 vol%)	300 ºC	No response
		350 ºC	No response
		400 ºC	No response
1.0 mol% Ag-loaded TiO_2	C_2H_5OH (0.10 vol%)	300 ºC	~3.15
		350 ºC	~5.28
		400 ºC	~13.0
1.0 mol% Ag-loaded TiO_2	SO_2 (0.050 vol%)	300 ºC	No response
		350 ºC	No response
		400 ºC	No response

Table 3.2 (Cont.) Summary of gas sensing performances of unloaded TiO_2 and metal-loaded TiO_2 sensor synthesized by FSP

Materials	**Gas concentration**	**Temp.**	**Response ($S=R_a/R_g$)**
2.0 mol% Ag-loaded TiO_2	H_2 (1.0 vol%)	300 ºC	~4.84
		350 ºC	~5.02
		400 ºC	~2.70
2.0 mol% Ag-loaded TiO_2	$(CH_3)_2CO$ (0.20 vol%)	300 ºC	~31.4
		350 ºC	~74.1
		400 ºC	~19.4
2.0 mol% Ag-loaded TiO_2	CO (0.10 vol%)	300 ºC	No response
		350 ºC	No response
		400 ºC	No response
2.0 mol% Ag-loaded TiO_2	C_2H_5OH (0.10 vol%)	300 ºC	~2.63
		350 ºC	~4.43
		400 ºC	~11.7
2.0 mol% Ag-loaded TiO_2	SO_2 (0.050 vol%)	300 ºC	No response
		350 ºC	No response
		400 ºC	No response

Table 3.2 (Cont.) Summary of gas sensing performances of unloaded TiO_2 and metal-loaded TiO_2 sensor synthesized by FSP

Materials	**Gas concentration**	**Temp.**	**Response ($S=R_a/R_g$)**
3.0 mol% Ag-loaded TiO_2	H_2 (1.0 vol%)	300 ºC	~2.48
		350 ºC	~4.36
		400 ºC	~1.71
3.0 mol% Ag-loaded TiO_2	$(CH_3)_2CO$ (0.20 vol%)	300 ºC	~27.2
		350 ºC	~50.6
		400 ºC	~18.6
3.0 mol% Ag-loaded TiO_2	CO (0.10 vol%)	300 ºC	No response
		350 ºC	No response
		400 ºC	No response
3.0 mol% Ag-loaded TiO_2	C_2H_5OH (0.10 vol%)	300 ºC	~1.40
		350 ºC	~2.02
		400 ºC	~9.45
3.0 mol% Ag-loaded TiO_2	SO_2 (0.050 vol%)	300 ºC	No response
		350 ºC	No response
		400 ºC	No response